Atmospheric Infrared Sounder (AIRS) Level 2 Simulation System Description Document

Evan Fishbein
Sung-Yung Lee
Eric Fetzer

14 May 2001

Version 1.0

Jet Propulsion Laboratory
California Institute of Technology
4800 Oak Grove Dr.
Pasadena, CA 91109-8099

JPL Document D-20316

Atmospheric Infrared Sounder (AIRS) Level 2 Simulation System Description Document

Prepared by:

E. F. Fishbein — Date

Approvals:

M. R. Gunson
AIRS Deputy Team Leader — Date

Contents

List of Figures

List of Tables

1 Introduction

The Atmospheric Infrared Sounder (AIRS) science team is developing algorithms for estimating geophysical parameters (Level 2 products) from observed upwelling thermal infrared and microwave radiances (Level 1B products). These algorithms are collectively referred to as the AIRS Core Retrieval System (ACRS). They will be delivered to the Earth Science, Data and Information System (ESDIS) component of the Earth Observing System (EOS) where geophysical parameters will be routinely produced. In support of these activities, the AIRS science team has developed the AIRS Level 2 Simulations System (AL2SS). This document describes the purpose and implementation of AL2SS.

AL2SS is one component of the AIRS simulation system. Simulation and data processing systems are shown in Figure 1. The left side shows the simulated data flowing from the highest level downward. The

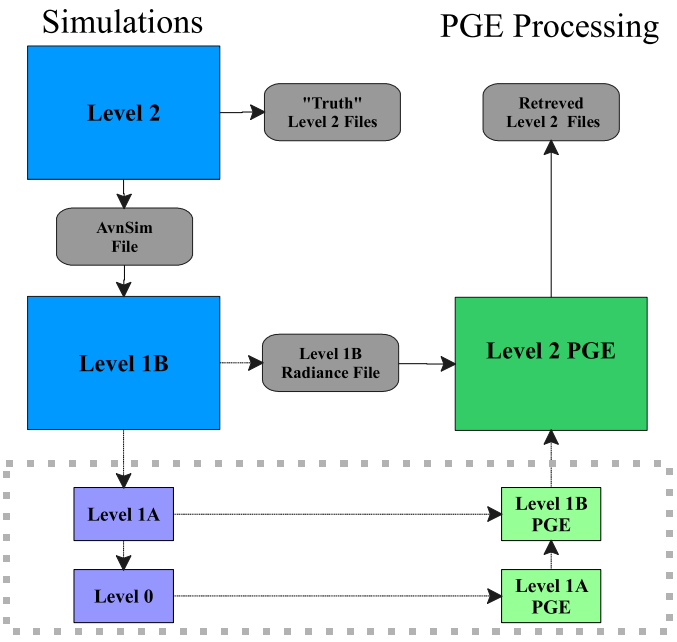

Figure 1: Data flow through the simulations and processing systems.

right side shows data flow through the AIRS Product Generation Executives (PGE). Rectangles represent processes, oval represent generated data products and arrow indicate flow direction. AL2SS generates geophysical state data (AvnSim and “truth” products), the Level 1B simulation (AIRSBT) generates calibrated radiances mixed with geolocation data and quality assessment (RadSim), Level 1A simulation generates raw products, e.g. uncalibrated radiances and the Level 0 simulation generates packeted data. At each processing stage the outputs of the simulation system and PGEs can be compared. The amount of difference between simulated and processed data (closure) is computed along any of the possible closed loops.

RadSim from AIRSBT are input to ACRS on the processing side of Figure 1. ACRS employs statistical and physical inversion methods to arrive at a solution consistent with observations. The fundamental problem of retrieval theory is the null-space issue which is concerned with finding the best solution from an

ensemble of solutions, all of which predict the radiances within the expected error budget. A description of the algorithms can be found in the AIRS Level 2 Algorithm Theoretical Basis Document [Chahine, 1998].

AL2SS produces an ensemble of geophysical states which represent the range of conditions AIRS will observe in operation. The output from ACRS is an estimate of the original ensemble. Statistical comparisons of differences between the AL2SS and ACRS products are used to assess quality of the ACRS product. AL2SS uses global weather forecasts, climatologies and other geophysical data sets. But hypothetical models and approximations are required to produce states with the required complexity.

The purposes of the Level 2 simulations are

1. retrieval algorithms development
2. error assessment of derived geophysical parameters
3. data system development and throughput assessment
4. development and testing of validation techniques.

The basic requirement of ACRS is the processing of the output of AIRSBT. Retrieval algorithm development further requires some degree of realism in the observations. The applicability to real data of the developed algorithms depends partly on the realism of the simulation. Error assessment in the simulations involves comparing AvnSim with quantities retrieved by the Level 2 PGE. Data system development requires sufficiently large amounts of data to exercise all components of the AIRS Team Leader Science Computing Facility (TLSCF). The development and testing of validation techniques requires corresponding correlative data, either real or simulated.

The use of simulated data for error assessment has been scrutinized in the past because of the potential to underestimate error sources, or miss error sources completely. However it has several advantages that make it a valuable contributor. Error assessment using simulated data is considerably simpler than validation using correlative data. Simulation data is perfect, i.e. “truth”, while real correlative data has its own error sources. Real data is never coincident and colocated, nor does it possess the same spatial sampling. Simulated data is more plentiful than correlative data and simulated data exists before real data becomes available. Finally simulated data can be perturbed in controlled experiments that are not possible with real data. Global simulated data have typical shortcomings of smaller overall variability than observations, and unrealistic small- scale smoothness from the limited resolution of the models used to generate then.

The various requirements place conflicting constraints on AL2SS. ACRS development requires simulation system stability so that changes in the retrieval software can be distinguished from those in the simulations. Error assessment and validation activities require realism, which implies simulation system development and evolution. Finally, the simulated time period needs to change to span new correlative data sets as they are included in validation activities. While AL2SS has limited realism to maintain stability, the simulations continue to evolve and become more complicated. This document describes version 2.15 of AL2SS as of January 2001 but does not document how it has evolved.

The remainder of this section describes basic simulation characteristics of geometry and timing. The state is defined as the combination of the geophysical and instrument states, and is the set of parameters needed to calculate a radiance. The retrieved state is a simplified geophysical state, characterized by the geophysical parameters returned by ACRS. Appendix A list the parameters modeled by AL2SS. A footprint is defined as the instrumental view projected through the atmosphere to the surface.

The AIRS investigation consists of three instruments: AIRS itself, the advanced microwave sounding unit (AMSU) and the Brazilian Humidity Sounder (HSB). AMSU has two separate units, AMSU-A1 and AMSU-A2 and three scan mirrors. AMSU has a field of view (FOVS) with a half-power width of 3.3°,

while HSB has a FOV with a half-power width of 1.1° and AIRS has FOV half-power width of 1.1°. The three instruments cross track scan at rates of 1 scan per 8 seconds for AMSU and 3 scans per 8 seconds for AIRS and HSB. A scanset consists of the 3 AIRS scans, 3 HSB scans and 1 AMSU scan that occur during an 8 second interval and cover the same ground swath. Two distinct scan methods are used by the three instruments: AMSU employs a stop-and-stare scan, while AIRS and HSB rotate at constant rates while viewing the earth. Also, off-nadir AMSU FOVs are not centered on associated AIRS and HSB FOVs. The scan are aligned so that the FOVs are arranged in a "golfball" pattern as shown in Figure 2. ACRS operates on groups of 19 FOVs (9 AIRS, 1 AMSU and 9 HSB). Each group is called a retrieval set and ACRS returns one state for each retrieval set.

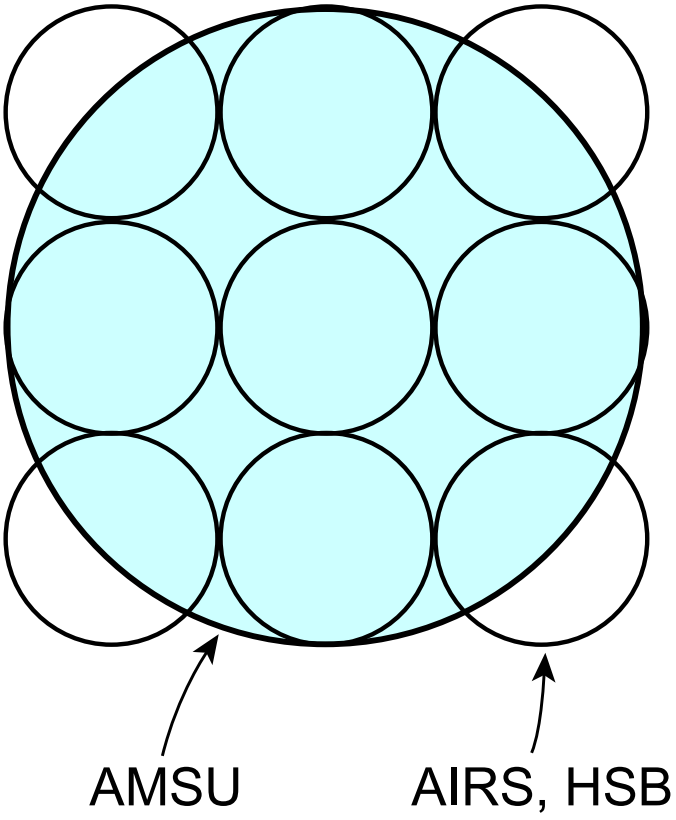

Figure 2: The alignment of AIRS, AMSU and HSB footprints constituting a retrieval set.

The details of the FOVs and scan determine the ensemble of geophysical states observed in one footprint. Actually each channel of AMSU, HSB and AIRS have a slightly different FOV and therefore observe a slightly different ensemble. The radiance observed by AMSU channel is an area-weighted average over its FOV, whereas the radiance observed by na AIRS and HSB channel involves an area weighted average convolved over the slew of the scan mirror. A more realistic simulations would generate an ensemble of states for each footprint and AIRSBT would average radiance depending on the scan characteristics of each instrument. Such complexity is unnecessary because of the poor spatial resolution of the input data and is

not included in the simulation. Instead, one geophysical state is generated for each AIRS footprint at its nominal center. The simulation system thus assumes that earth and atmosphere are homogeneous over the AIRS FOV. HSB is assumed to observe the same mean state, and AMSU is assumed to observe the mean of the 9 AIRS states. This approximation is poorest at aft nadir scan angles, but still insignificant.

2 Data Flow

The simulations are processed one granule at a time and involve four separate processes. The names and order of processes are shown in Figure 3. Nine input data types are used by the simulator. Two intermediate outputs and two final outputs files are created.

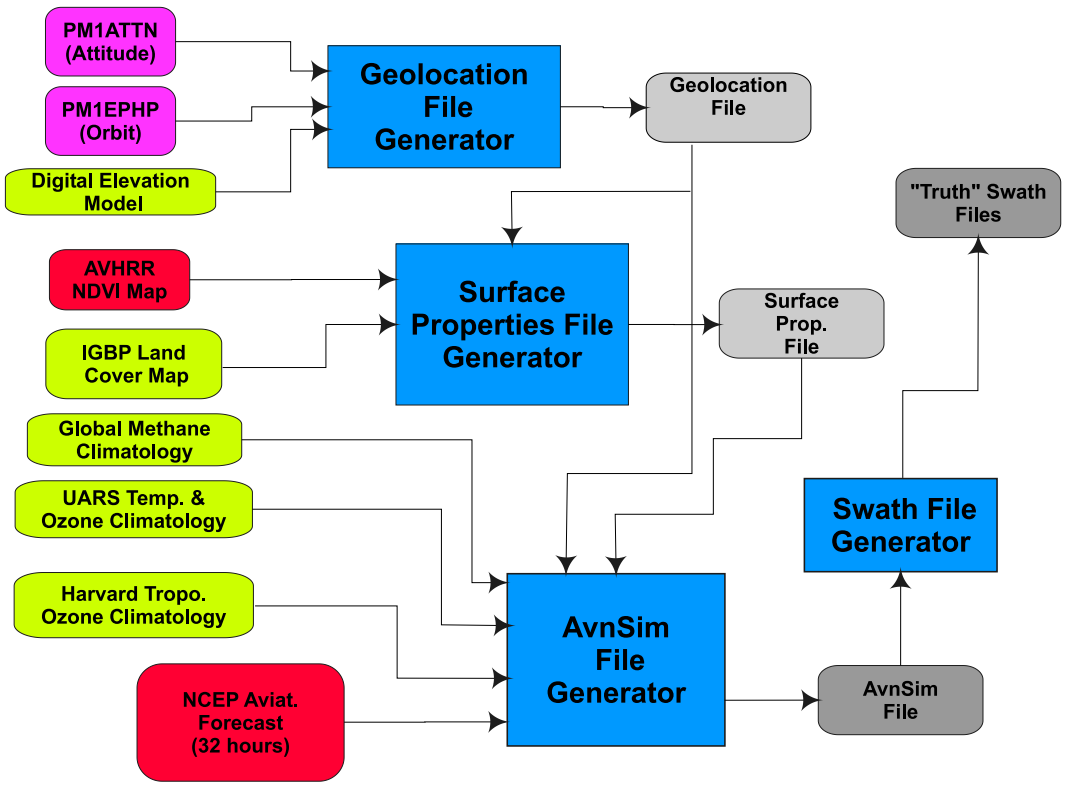

Figure 3: Data Flow into the simulation system. Processes are shown as square boxes, data as ovals. Blue boxes are separate processes, magenta boxes are day-specific inputs from Aqua flight dynamics facility (or its simulation), red boxes are day-specific geophysical inputs, green boxes are invariant inputs such as maps and climatologies, and gray boxes are outputs. Light gray boxes are intermediary outputs.

Input to the simulation includes satellite specific data, NCEP aviation forecast files, numerous climatologies and digital geographic maps (DGM) and images. Generally these data sets are global and provide a reasonable ensemble of global variability. However they do not have sufficient spatial resolution to model variability between AIRS footprints within a retrieval set. This local variability is important to the AIRS

investigation and must be present in the simulation system in order to estimate cloud properties and clear sky radiances. In the absence of an external estimate of local variability, AL2SS applies random perturbations to the 9 states contained in a retrieval set. This model of local variability may be most significant for its lack of realism in the simulation system, especially for its impact on error assessment of ACRS. The surface properties generator provides parameters characterizing surface infrared radiative properties and was introduced to AL2SS to provide more realistic local variability.

2.1 Geolocation Simulator

The geolocation file generator process (GeoSim) creates all instrumental state parameters contained in the Level 2 simulation. These include all pointing, satellite location, solar ephemeris and geolocation parameters and are nominally generated in Level 1A processing. The underlying code and algorithms are extracted from the Level 1A PGE and are therefore consistent with it. Most of the computations are performed by routines in the EOS Science Data Processing (ESDP) Toolkit Geolocation Package. Details concerning definitions and algorithm used in GeoSim can be found in geolocation package Algorithm Theoretical Basis Document [Noerdlinger, 1995], or in the Level 1B software.

The inputs to GeoSim are a simulated orbit ephemeris file (PM1EPHP) and simulated attitude file (PM1ATTN). PM1EPHP is generated with the EOS Core System (ECS) Spacecraft Orbit Simulator. The orbit simulator uses adjusted orbit elements (listed in Table 1) which approximately produce a sun-synchronous orbit with an 1330 local time ascending equator crossing. The orbital dynamics contained in the simulator are approximate and result in a drift of the equator crossing time if integrated for longer than a few weeks. Therefore the orbit elements (including the launch time) are adjusted for each simulation period. The satellite attitude is constrained to be along the orbit, therefore roll, pitch and yaw are all zero.

Orbit Element	Value
Semi-major axis	7,077,590 m
Eccentricity	0.0012
Inclination	98.1450°
Right ascension of ascending node (RA)	272.348°
Argument of perigee (AP)	90.0°
Mean anomaly at launch	270.0°
Rate of change of RA	1.1348×10^{-5} °/s
Rate of change of AP	0.0°/s
Mean motion at launch	0.060733°
Period	5927.55 s

Table 1: Simulated orbit elements for a mid December 2000 simulation period.

Footprint position is evaluated from the AIRS viewing angle relative to the platform coordinate system and the time of the measurement. Time is nominally reported in seconds of secTAI93 (seconds Temps Atomique International, 1993 epoch), the incremented number of seconds UTC since midnight on 1 January 1993. Seconds of secTAI93 (hereafter abbreviated as TAI time) differ from UTC time by the leap seconds added to UTC time to correct for day length varying from 86400 s.

The simulated AIRS scan is synchronized to 0 TAI, and each granule of data starts on an integer multiple of 360 seconds. The midpoint of the first footprint occurs 504.202 ms later and subsequent footprints occur every 22.15 ms. This approximates the true AIRS scan to within a few milliseconds. The scan has 90 footprints symmetric around nadir. Therefore the first footprint views -48.95° off AIRS nadir. AIRS is assumed to be aligned with the EOS PM1 satellite- centered coordinates, so the nadirs of AIRS and EOSPM1 are parallel. The positions of the instrument and sun relative to the footprint are also provided by the toolkit. The calculations include contributions from the oblateness of the earth's spheroid, aberration due to motion of the instrument relative to the ground, and earth rotation during the travel of light from the surface to the instrument. The location of the center of the footprint on the ground is correct to less than 75 m.

Land fraction and surface elevation and their errors are integrated quantities evaluated by sampling a DGM over the area an AIRS FOV projects onto the surface. Individual rays along the edge of the FOV are projected onto the ground to map the extent of the footprint. The DGM contains elevation and surface type and has $30''$ spatial resolution. Elevation is relative to the WGS84 Geoid, while the surface type model indicates land, ocean, inland water or coastline. The number of DGM pixels in the FOV becomes excessive large near the poles for fixed angular sampling. Therefore an approximate fixed area sampling algorithm was adopted that uses around 100 values per footprint and depends on latitude and view angle.

The output of GeoSim is an ASCII file of footprint and granule geolocation data. The footprint data is listed in Table 12 of Appendix A. The granule information includes the start time, stop time and position of the satellite at the beginning and end of the granule, the type of orbit segment (e.g. day or night, ascending, descending or polar), orbit number since launch, and the most recent equator crossing time and longitude. The granule information propagates into the attributes and metadata of AIRSBT and ACRS data products.

2.2 Surface Properties File Generator

The surface properties file generator is an intermediary process that adds local variability to surface properties. The surface properties file is generated from the GeoSim output file, a composite gridded AVHRR image of normalized difference vegetation index (NDVI) and a map of International Geosphere Biosphere Programme (IGBP) surface classification. The surface properties file describes the composition of the surface within each footprint.

2.3 Aviation Forecast Simulator

The AvnSim file generator collects instrumental, geolocation and geophysical state parameters sufficient to generate radiances for each footprint. Input data include the GeoSim output, surface properties file, forecasts and climatologies. The climatologies include temperature and O_3 from the UARS project climatology, CH_4 from the ATMOS investigation and CO from the US standard atmosphere.

These data combined with models of geophysical variability are interpolated to the time and location of the footprint and place on a standard vertical grid. This grid has 100 fixed pressure levels from 1100 hPa to 0.016 hPa and is referred to as the AIRS 100 level internal grid (an implied level 101 at 0 hPa extends the grid to the top of the atmosphere, but is trivial because the overlying layer is homogeneous). The output file (AvnSim) is a binary file of fixed length records containing one record per footprint, preceded by a granule-specific record. The file format is described in Appendix A. The details of algorithms in the AvnSim file and surface properties file generators are described in latter sections.

2.4 Level 2 Product Generator

The Level 2 product generator takes as input the AvnSim file and generates files having the same format as Level 2 PGE output files. These are the EOS HDF formatted AIRS Level 2 standard and support products files. Profiles in the support files are on the AIRS 100 level grid. Constituent profiles are in layer amount (molecules/cm^2) and air temperature is the point value at the pressure level. Profiles in the standard files are on a 28 level pressure grid from 1100 hPa to 0.1 hPa. The standard products are the core AIRS retrieval products and include air temperature, H_2O vapor mass mixing ratio and O_3 volume mixing ratio. Within the level 2 PGE, standard profile products are derived from corresponding support products, e.g. O_3 mixing ratio from O_3 layer amount. The software used in the Level 2 product generator are extracted directly from the Level 2 PGE and therefore 100% consistent.

Geophysical parameters are defined once per retrieval set in the Level 2 PGE products, but once per AIRS footprint in the AvnSim files. Cloudiness however is defined once per AIRS footprint in both files. The Level 2 product generator first decimates the AvnSim file, selecting the center state from each retrieval set. Cloudiness is obtained from all nine footprints, but the other cloud properties are from the center footprint only. When all the footprints in a retrieval set have the same cloud layers, the cloud properties from the center footprint provide a reasonable description of the clouds in the other footprints. However when this is not the case, the association between cloudiness and other properties can be incorrect in the Level 2 files. Sometimes the retrieval set contains more than two cloud layers or the center footprint has fewer layers than other footprints. In these cases the cloud properties in the simulated Level 2 files do not provide an accurate description of the clouds layers in the retrieval set (or the AvnSim files and the radiances). Similarly, surface properties may not accurately be characterized in the Level 2 files, especially over land. Section 7 contains an analysis of parameter variability within retrieval sets. Parameters with large variability are not accurately characterized in the Level 2 files.

3 Data Sets

In this section, the data used in the simulation system are described. These include the NCEP global aviation forecasts, the UARS climatology, the Harvard tropospheric ozone climatology and the AVHRR composite NDVI imagery.

3.1 Aviation Forecast

The NCEP global operational aviation analysis and forecast (AVN) files are processed four times daily at 0 UT , 6 UT, 12 UT and 18 UT. Each processing produces an analysis (0 hour forecast) and forecasts every three hours nominally for at least 72 hours. The analysis is initialized by the 6 hour forecast from the previous run and contains a subset of the forecast fields. Because the analyses do not contain the three cloud fields, they are not suitable for the simulations and are not used. The output grid has a 1 $^\circ$ longitude by 1 $^\circ$ latitude resolution and vertical pressure grid, although other vertical grids (e.g. sigma coordinates and tropopause) are present.

The fields used in the simulation are:

surface properties: pressure, geopotential height, skin temperature and albedo

dynamics: winds at 10 meters above the surface

profiles: temperature, relative humidity and O_3 mass mixing ratio

clouds: low, middle and high cloudiness, base and top pressure

Temperature, relative humidity and O_3 profiles are defined on 26, 21 and 6 levels listed in Table 2. A complete list of forecast fields is provided in Appendix B.

	Pressure (hPa)																								
Species	10	20	30	50	70	100	150	200	250	300	350	400	450	500	550	600	650	700	750	800	850	900	925	950	975	1000
Temp.	X	X	X	X	X	X	X	X	X	X	X	X	X	X	X	X	X	X	X	X	X	X	X	X	X	X
R.H.						X	X	X	X	X	X	X	X	X	X	X	X	X	X	X	X	X	X	X	X	X
O_3	X	X	X	X	X	X																				

Table 2: Pressure levels for forecast temperature, relative humidity and ozone profiles. An X indicates a valid level.

For each footprint, parameters are interpolated from the grids using several linear interpolations. The grid is first interpolated to the footprint time using forecasts from the same run. For example, a footprint at 0430 UT would use the 3 and 6 hour forecasts from the 00 UT run. Next a bilinear interpolation is applied within the 1° by 1° rectangle containing the center of the footprint. Lastly, if the parameter is a profile, a vertical interpolation to the AIRS standard grid is applied.

Each footprint sees an average state previously described.. In principal the bilinear interpolation could be applied for an ensemble of points in the footprint to arrive at a footprint-mean value. However, a footprint contains approximately 2% of a model grid rectangle and most model fields very slowly between grid points. Samples within a footprint are very nearly identical and using the value at the center is a good approximation for the footprint mean. An assessment of variability between neighboring footprints provides a measure of grid box variability and is discussed in Section 7.

3.2 UARS Climatology

The UARS climatology was created prior to the launch of the Upper Atmosphere Research Satellite in September 1991. We use a version provided by the UARS Microwave Limb Sounder (MLS) science team, with some previously missing high-latitude regions filled. It consists of monthly and zonally averaged means and variances of temperature and 18 species including, H_2O, O_3, CH_4 and CO. The climatology has 17 10° wide latitude bins from -85° S to 85° N centered on -80° S, -70° S .... Included are means for day, night sunrise and sunset local conditions. Species climatologies are in units of dry volume mixing ratio. Temperature has 43 levels from 900 hPa to 0.000025 hPa and O_3 has 31 levels from 900 hPa to 0.005 hPa; AIRS simulations use the O_3 and temperature day time climatologies.

Two monthly climatologies are linearly interpolated to the time of the footprint. The climatologies are assumed to represent the state at 12 UT on the 15th of the month. Linear interpolation in latitude is next applied to arrive at profiles at the latitude of the footprint. In the winter high latitude stratosphere and mesosphere, the polar vortex is often displaced from the pole, and O_3 and temperature have large zonal variability which is not accurately represented in the zonal-mean climatology. Therefore temperature and O_3 profiles from the UARS climatology do not constitute a representative ensemble of stratospheric and mesospheric conditions in the winter at high latitude.

3.3 Harvard Tropospheric Ozone Climatology

The Harvard climatology [Logan, 1998] contains monthly tropospheric ozone values from pole to pole with 5° longitude bins and 4° latitude bins on 13 pressure levels at 100, 125, 150, 200, 250 and 300 to 1000 hPa in 100 hPa intervals. A similar interpolation schemes described in the previous sections is used to

generate a profile at the footprint location. An error in the latitude interpolation results in a weak horizontal gradient within each $5^\circ \times 4^\circ$ bin; this has been corrected in the Version 2.2 simulation system.

3.4 AVHRR NDVI Data

Local variability is added to the surface properties with a composite AVHRR normalized difference vegetation index (NDVI) image [Eidenshink and Faundeen, 1994. The images were produced at the USGS Eros Data Center for the period from April 1992 through May 1996. Composites were derived from 10 days of AVHRR scenes filtered for cloud-free pixels. The filtered data were mapped onto an Interrupted Goode Homolosine projection (shown in Figure 4). The image has equal area 1 km^2 pixels. The December 2000 simulations used the image from 11 December 1995 and the previous simulation period (13-14 September 1998) used the image from 11 September 1993 (both are shown in Figure 4). More recent images are available from the Goddard DAAC for 13 July 1981 through March 2001, but this data is coarser with only 8 km resolution.

NDVI is not determined over water or for low light conditions (solar zenith angles greater than 80°). Pixels over water are flagged "over water" while low light pixels over land are flagged "undefined"; NDVI of undefined pixels is set to zero. The black regions on the December image poleward of 55° N show the extent of low light conditions during winter.

4 Profile Generation

This section describes how the temperature, water vapor, liquid water and trace gas profiles are generated. The section begins with a description of the vertical interpolation and "joining" procedures.

4.1 Vertical Interpolation and Averaging

Input profiles are interpolated to the AIRS 100 level pressure grid by a single routine using linear interpolation in the logarithm of pressure. Input profiles not spanning the grid are extrapolated to cover the full range with a profile-dependent minimum-value constraint applied.

Several methods of extrapolation have been adopted and consist of using:

1. A constant equal to the value at the end point.
2. A constant equal to the average of the end point and the adjacent point.
3. A linear extrapolation.
4. A linear extrapolation limited to 10 times the difference between the end point and its neighbor.

Method 3 is preferred over method 1,. Least preferred are methods 2 and 4, used when conditions at the end points, such as anomalous values or lapse rates, do not allow the other methods. The type of extrapolation depends on profile type and is listed in Table 3 for each profile. The most realistic results occur only when the amount of extrapolation is limited by combining data with complementary vertical ranges from several sources.

'Joining' is the procedure for combining profiles. Joined profiles are weighted averages of two or more extrapolated profiles where each profile is given greater weight in the region where it is more realistic. Profiles are averaged in pairs. The pressure level where the profiles have equal weight is referred to as the

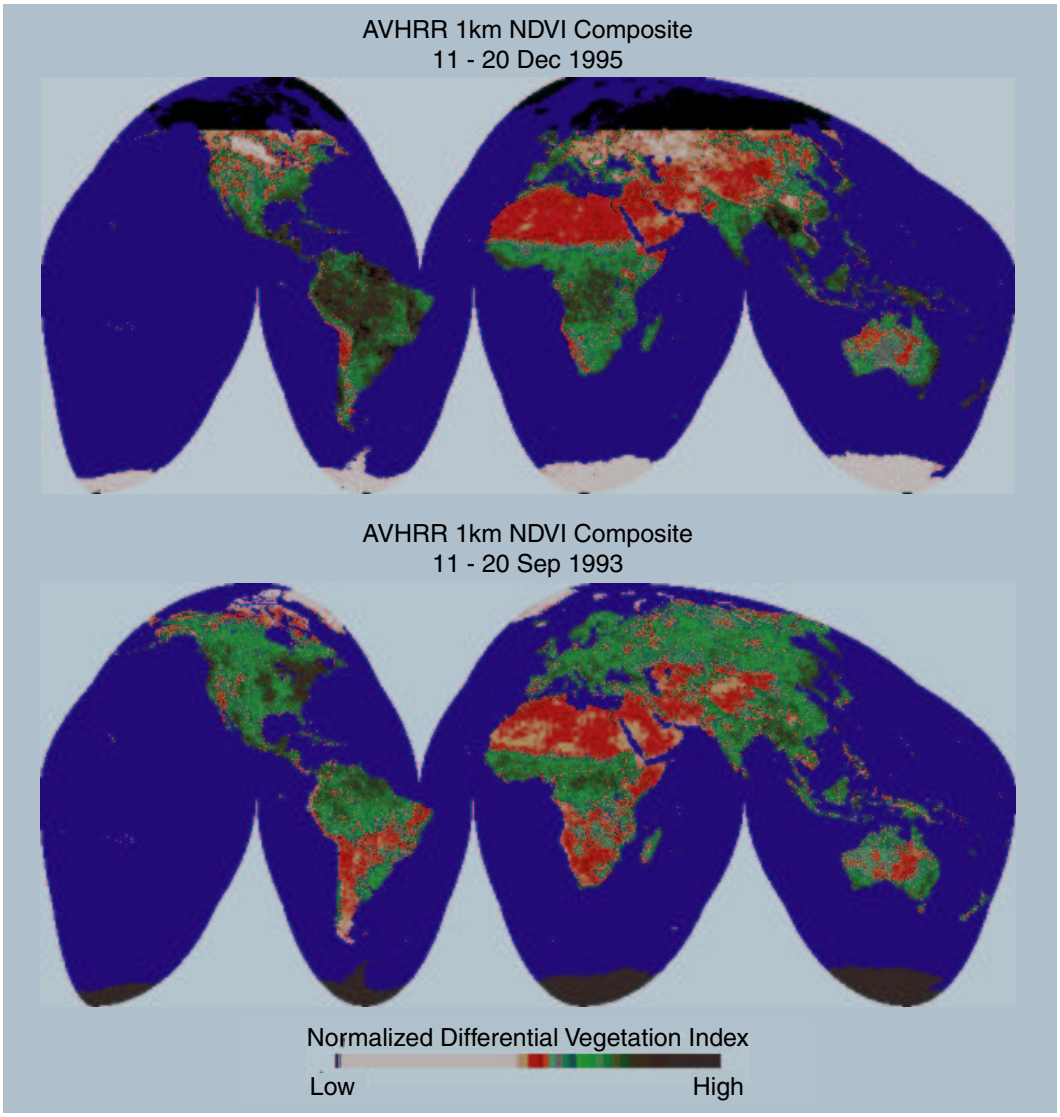

Figure 4: Composite NDVI Image for 11-20 December 1995 and 11-20 September 1993

tie point P^* and the weights exponentially approach 1 and 0 away from P^*. The weighting function f depends on the log pressure normalized by a scale height H and is given by:

$$f(p) = \frac{1}{2}\left\{1 - \tanh\left[\frac{\log_{10}(P/P^*)}{H}\tanh^{-1}0.9\right]\right\} .$$

The weight decay to 0.05 one decade of pressure from the tie point.

Quantity	Method Bottom	Top	Transformation	Lower Bound
Air Temperature	3	3	K	none
Humidity	3	-	$\log(\mathrm{mmr})$	3×10^{-6}
Liquid Water	2	2	$\log(\mathrm{mmr})$	3×10^{-8}
Ozone (AVN)	3	1	$\log(\mathrm{vmr})$	1×10^{-9}
Ozone (Logan)	4	4	$\log(\mathrm{vmr})$	1×10^{-9}
Ozone (UARS)	3	1	$\log(\mathrm{vmr})$	1×10^{-9}

Table 3: Extrapolation procedures by parameter. Method number refers to the extrapolation methods listed above, transformation refers to a change of variable prior to interpolating/extrapolating and the units of the input profile, e.g. Kelvin (K), mass mixing ratio (mmr), or volume mixing ratio(vmr). Lower bound refers to the minimum allowed value.

4.2 Air Temperature

Air temperature is derived from the AVN file and the UARS temperature climatology. The profiles are combined with a tie point at 10 hPa and a scale height of 1 pressure decade. Figure 5 shows a sample result. It follows the forecast below 10 hPa and smoothly transitions to the climatology profile above it.

4.3 Water Vapor

Water vapor is output as layer column amount in molecules/cm^2. The AVN forecast files contains profiles of relative humidity on 12 levels between 1000 hPa and 100 hPa. Relative humidity RH is converted to mass mixing ratio using the approximation $RH \approx X_{\mathrm{H_2O}}/X^{Sat}_{\mathrm{H_2O}}$ where $X_{\mathrm{H_2O}}$ is the dry mass mixing ratio of water vapor (RH is the ratio of wet volume mixing ratios). The saturation mass mixing ratio is computed from a functional fit in the Smithsonian Meteorological Tables [List, 1958].

The profiles is extrapolated upward using a power law:

$$X_{\mathrm{H_2O}}(P) = X_{\mathrm{H_2O}}(P^T)^{(P/P^T)^3}$$

where P^T is the pressure at the top of the profile, in this case 100 hPa. The conversion from volume mixing ratio to layer amount (in molecules/cm^2) is $10^4 A \Delta P / M g_0$ where is ΔP is the pressure difference across the layer in Pa, M is the mean molecular mass of dry airs in kg/g-mol, A is Avogadro's number, and g_0 is a constant gravity (9.80665 m/s^2). Variations in the mean molecular weight of airs, such as those associated with water vapor variability or changes in gravity with latitude and height are not included in the calculations.

Figure 6 shows a sample profile compared to UARS water climatology. The climatological water vapor mixing ratio is approximately constant throughout most of the stratosphere owing to the absence of sources and weak vertical transport. The winter high latitude profile can have larger gradients owing to stronger vertical transport in the winter polar vortex, but even there, the simulated profile is not realistic. Therefore, water vapor sensitivity studies above 100 hPa are not possible with this simulation.

4.4 Ozone

The ozone simulations must be realistic throughout the troposphere and stratosphere. The forecast, however, includes O_3 from only 100 to 10 hPa. In the upper stratosphere and mesosphere, the UARS climatology

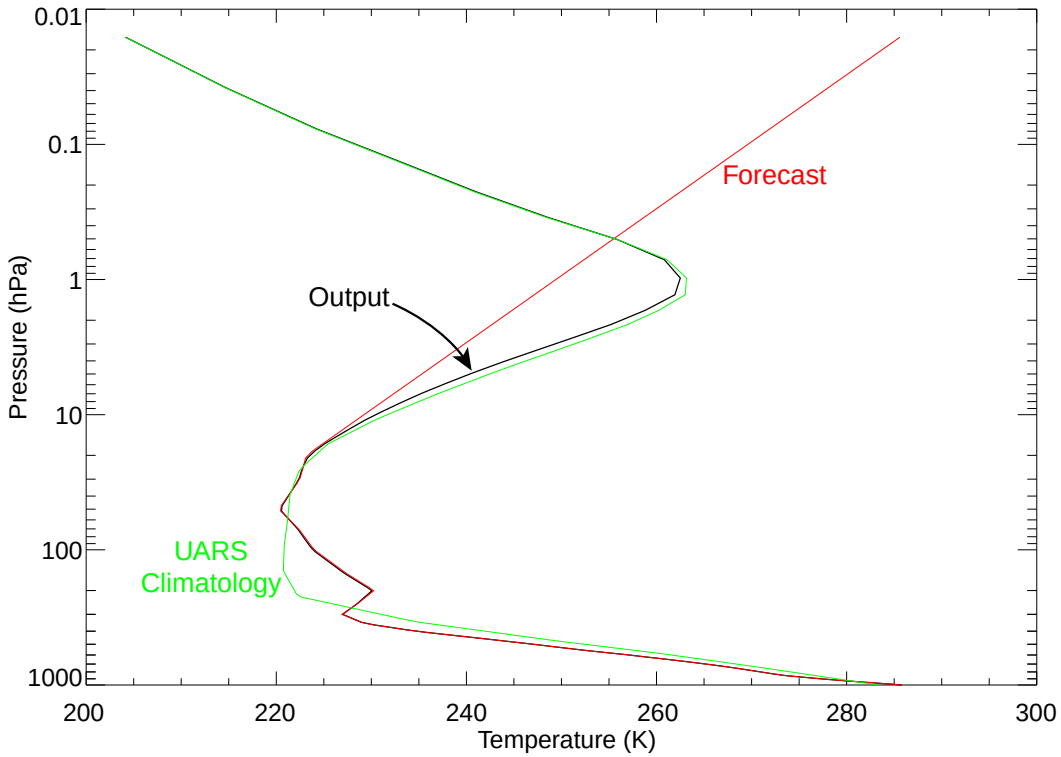

Figure 5: Representative temperature profile from the 13 September 1998 simulation, granule 31 at 0.77° E, 55.89° N. The Red curve is the AVN temperature profile, the green curve is the UARS climatology profile and the black curve is the combined profile.

provides the better estimate of O_3. The two are joined at 10 hPa (the top of the grid) with a scale height of 1 pressure decade. In the troposphere the Harvard climatology provides a better estimate than an extrapolation of the forecast. The extrapolated forecast is therefore joined to the Harvard tropospheric O_3 climatology at the tropopause with a scale height of $1/2$ pressue decade. The tropopause is define as the first level above 500 hPa where the lapse rate is less steep than -2 K/km. The conversion from volume mixing ratio to layer amount is as done for water vapor, except that the forecast O_3 profile has units of mass mixing ratio.

Figure 7 illustrates unusually large simulation ozone values from extrapolating the forecast into the troposphere. The lower panel shows an extrapolated forecast rapidly decreasing within the troposphere with an output profile closely follows the Harvard climatology. The upper panel shows a case where the lapse rate near the tropopause of the forecast is small and the extrapolated forecast profile is a factor of 10 to 100 larger than the climatology. The combined profile is significantly larger than the climatology, but not unrealistic. Anomalously large tropospheric O_3 profiles are therefore a possibility with this method, but none have been identified to date.

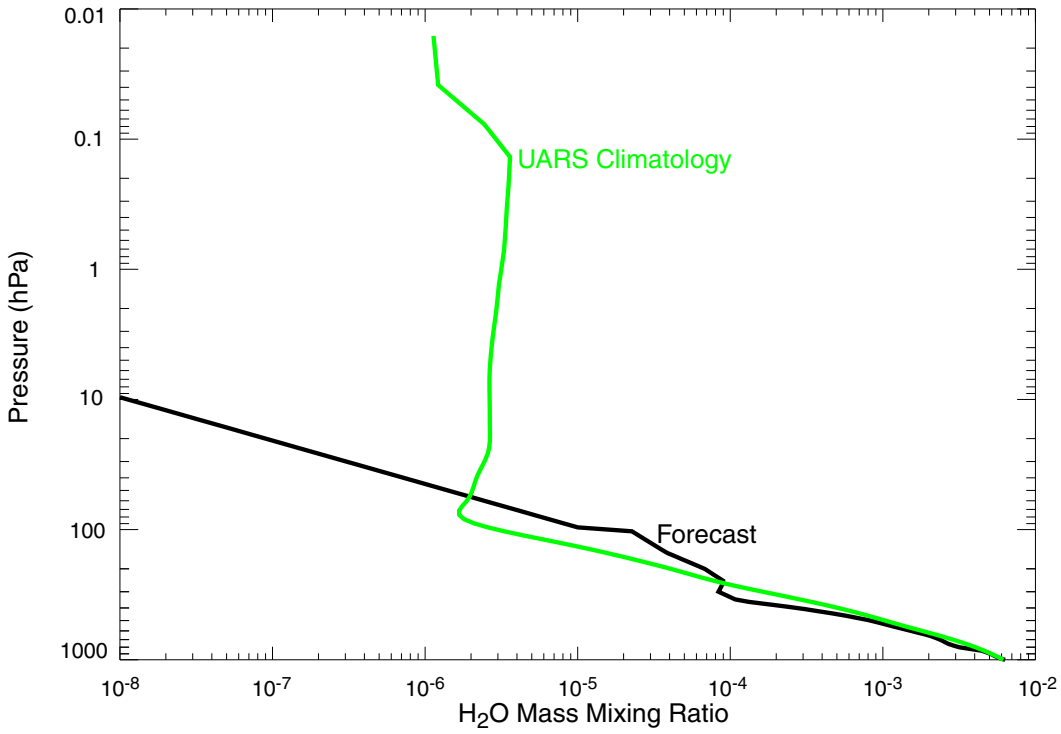

Figure 6: Representative water profile from Granule 31 at 0.77° E, 55.89° N on 13 September 1998. The Red curve is the extrapolated forecast water vapor profile. The green curve is the UARS climatology.

4.5 Methane

A single global mean methane profile is used for all footprints. The profile was provided by F.W. Irion [Gunson *et. al.*, 1990] from an analysis of ATMOS limb occultations. It is shown in Figure 8. Also shown is the U.S. standard atmosphere profile used as the regression basic state in the AIRS RTA. The profiles are in good agreement except in the mesosphere, but these differences have little impact on the spectrally-averages radiances observed by AIRS. Methane layer amount is derived from the mixing ratios using the approach described for water vapor.

4.6 Carbon Monoxide

The U.S. standard atmosphere CO profile is used. The AIRS RTA uses this as a reference and so CO produces no radiance perturbation from the RTA regression mean state. The profile is shown in Figure 9 along with the UARS climatology global mean daytime state.

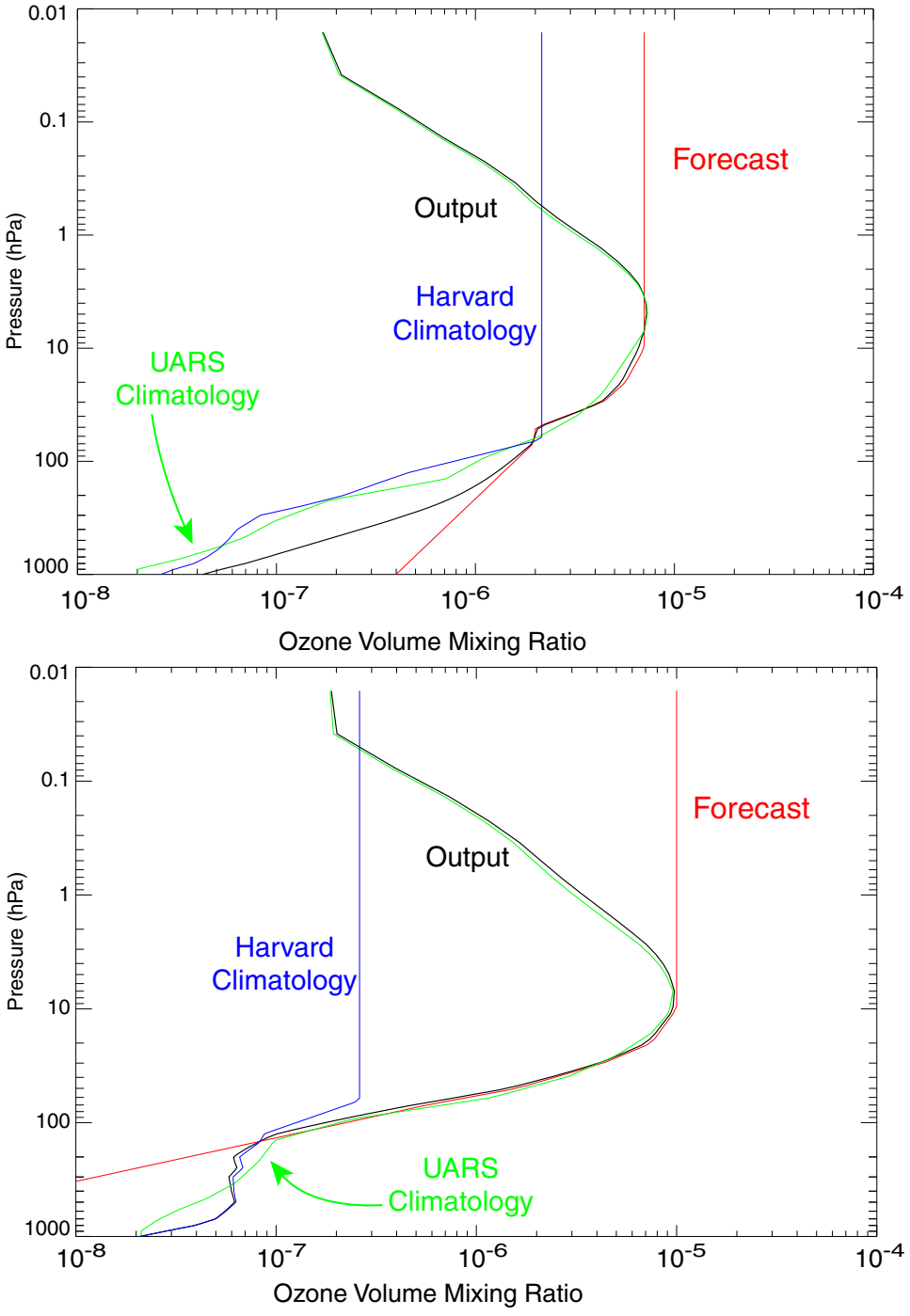

Figure 7: Ozone volume mixing ratio profile from the 13 December 1998. The upper panel is from Granule 31 at 0.77° E, 55.89° N. The lower panel is from Granule 108 at 29.75° E, 2.01° N. Red shows the forecast, green the UARS climatology, blue the Harvard climatology and black the combined profile.

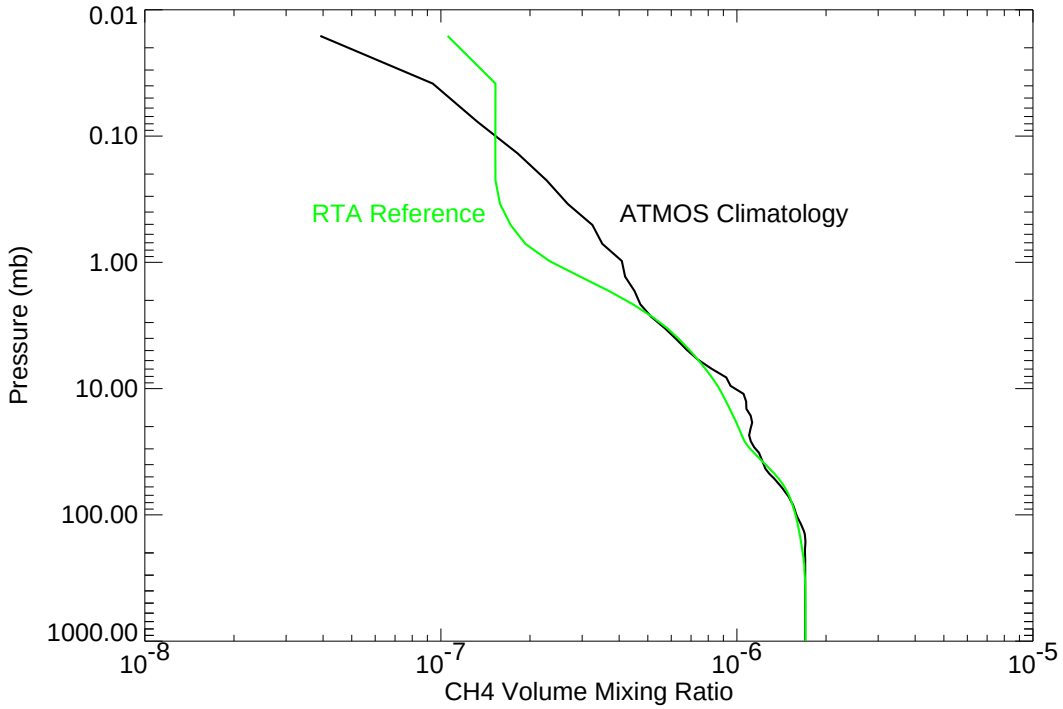

Figure 8: Global CH_4volume mixing ratio profile. The ATMOS climatology is in black, the U.S Standard Atmosphere in green.

4.7 Carbon Dioxide

The carbon dioxide simulation uses a model developed by S. Leroy for AL2SS based on measurements of CO_2 at ground stations and a realistic representations of meridional and vertical transport. The model includes a positive trend, seasonal variability and a surface source whose rate is slow compared to transport. The original model had very little variability during the September 1998 simulation so the phase and amplitude of the seasonal cycle were slightly modified to increase variability for that period. This modified model has been used since. The trend (X^{trend}) and seasonal (X^{seasonal}) terms are:

$$\begin{aligned} X^{\mathrm{trend}}_{\mathrm{CO_2}}(\theta) &= 331 \times 1.0041^{(T-1976)} \\ X^{\mathrm{seasonal}}_{\mathrm{CO_2}}(\theta, P) &= [7.9\,\mathrm{erf}\,(2\sin\theta) + 6.4\,]\sin\left(2\pi T - \pi/6\right)\,(P_0/P)^{0.4222}\,, \end{aligned}$$

where mixing ratios X are in ppmv, time T is in common years (from 0 CE), θ is the latitude in radians, pressure P is in hPa, the reference pressure P_0 is 1000 hPa and the exponent is the ratio of the CO_2 scale height (3.3 km) to the pressure scale height 7.817 km. Variability is largest in late winter and smallest in late fall. Although the AvnSim generator produces profiles of CO_2 amount, the output files contain only the pressure-weighted mean CO_2 mixing ratio

$$\bar{X}_{\mathrm{CO_2}} = X^{\mathrm{trend}}_{\mathrm{CO_2}}(\theta) + (0.4222/1.4222)\, X^{\mathrm{seasonal}}_{\mathrm{CO_2}}(\theta, P_0)$$

Figure 10 shows the latitude dependence of mean CO_2 volume mixing ratio for 13 September 1998.

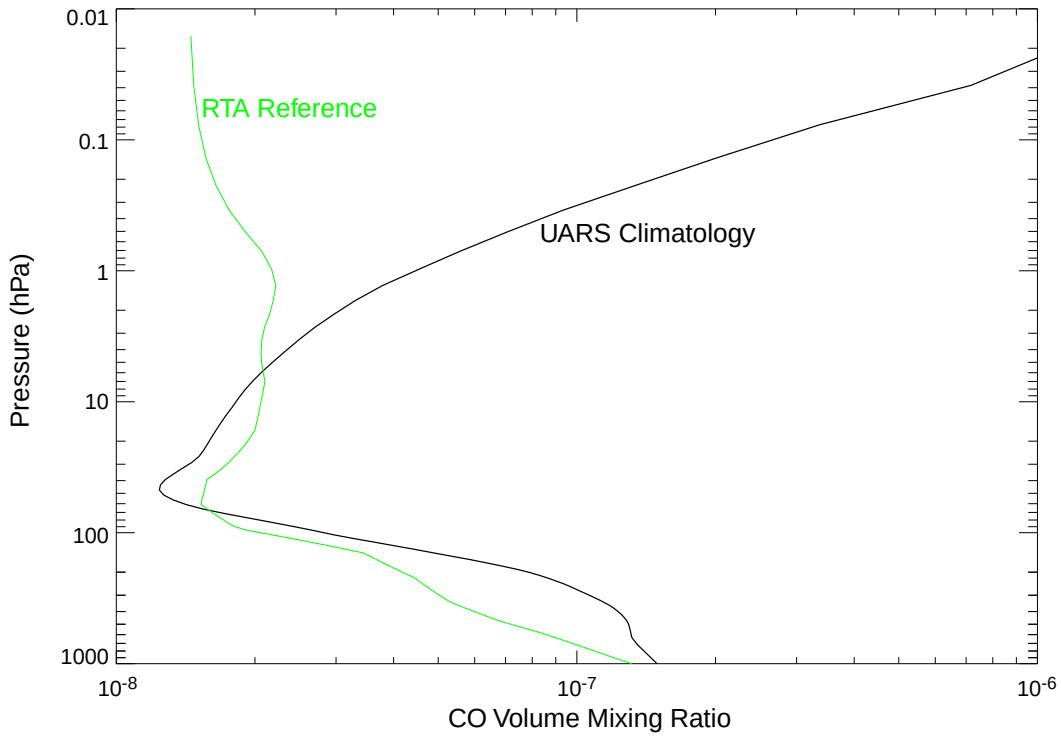

Figure 9: Global carbon monoxide volume mixing ratio. The profile used in the simulations is in black, the global mean UARS climatology in green.

5 Surface Properties

Surface properties include skin temperature, surface pressure, land fraction, topography and microwave and infrared emissivities and reflectivities. Surface skin temperature and surface pressure are obtained from the forecast as described above. Each surface grid point in the model is either land or water and is flagged as such in the output. However the simulation smoothly interpolates all fields within grid boxes. Therefore discontinuities across coast lines such as those in skin temperature are smoothed. Studies using simulation to develop geolocation validation approaches may be hampered by this.

Surface pressure P_s is the forecast model value P_{AVN} corrected for local topography assuming a dry adiabatic surface layer

$$P_s = P_{\mathrm{AVN}} \left[1 - \frac{g(a_s - a_{\mathrm{AVN}})}{C_p T_s} \right]^{\frac{C_p}{R}}$$

where a_s is the surface elevation, a_{AVN} is the model surface elevation, T_s is the surface air temperature, and C_p and R are the specific heats at constant pressure and the gas constant, both per unit mass.

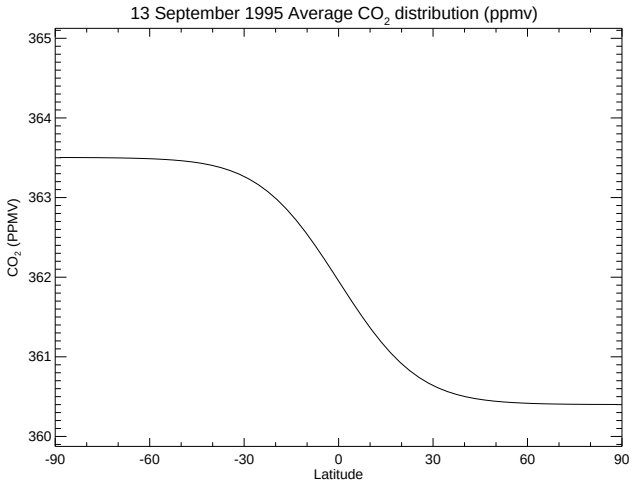

Figure 10: Dependence of mean carbon dioxide volume mixing ratio on latitude.

5.1 Microwave Surface Model

The microwave emissivity models employed by AL2SS and ACRS are designed to be consistent and invertible. The ACRS microwave retrieval determines surface emission, and from this estimates the skin temperature and emissivities assuming one of 6 emissivity models. AL2SS uses the same 6 emissivity models, however the method used to determine the emissivity model is different. Land fraction and ratios of radiances are used to assign a model in ACRS. AL2SS does not know the radiances and uses land fraction, skin temperature and latitude instead. No test has been performed to determine if the resulting radiances lead ACRS to identify the same model. The model surface types are land, sea water and four kinds of ice: first-year sea ice, multi-year sea ice, glacial ice and dry snow. The microwave surface class (MW_Class) indicates which model applies to each footprint. Table 4 lists the classes and criteria for assigning MW_Class to a footprint.

MW Class	Description	Land Fraction	Temperature	latitude
1	land	> 0.97	> 273.16 K	
5	snow		≤ 273.16	equatorward 70°
6	glacier			poleward 70°
2	sea water	≤ 0.97	≥ 271.2 K	
3	first year sea ice		265 K $< T <$ 271.2 K	
4	multi year sea ice		≤ 265 K	

Table 4: Microwave surface classes.

Footprints of MW_Class 1, 5 and 6 are composed of one component, "land", "snow" or "glacier ice" respectively. Class 2 footprints (sea water) contain both land and water, and the emissivity of each component is evaluated separately and combined according the land fraction. MW_Class 2 is further subdivided into two classes by the retrieval, depending on whether a footprint is 100% sea or has some contamination from land.

The two sea ice classes (3 and 4) contain either first-year or multi-year sea ice, plus sea water. When there is land in the FOV, its contribution to the radiance is ignored, assuming that any land in the footprint is covered by ice. The fraction of sea ice is a normally distributed random variate with a mean determined by the difference between the skin temperature T_s and nominal freezing temperature of sea ice (271.2 K). The mean $\hat{f}_{\text{seaice}}$ and standard deviation σ_{seaice} of the fractional ice amount are

$$\begin{aligned} \hat{f}_{\text{seaice}} &= \frac{1}{2}\left(1 + \tanh\frac{271.2 - T_s}{5}\right) \\ \sigma_{\text{seaice}} &= \hat{f}_{\text{seaice}}(1 - \hat{f}_{\text{seaice}}) \ . \end{aligned}$$

The ice fraction is constrained within [0, 1]. Its standard deviation is largest at 0.25 when the skin and ice freezing temperatures are equal. The standard deviation is 0 when the expected mean is 0 or 1. This model attempts to mimic variability arising from the kinetics of freezing and thawing acting to decorrelate skin temperature and sea ice amount.

The emissivity is specified by "hinge" point frequencies at 23.8, 31.4, 50.3, 89, 52.8, 150 and 183.31 MHz (stored in the AvnSim file in this order). Emissivity at other frequencies are linearly interpolated from this set. Figure 11 show the emissivity for each material at the microwave hinge point.

Land is assumed to be gray. The land model emissivities are uncorrelated random number from an normal distribution with a mean of 0.95 and a standard deviation of 0.025. They are limited to the range [0.85, 1]. The emissivities at 50.3 and 52.8 MHz are as uncorrelated as the emissivities at 23.8 and 183.31 MHz; this may lead to an unrealistically large variability.

Microwave emissivity of sea water is evaluated from a table indexed in AMSU scan mirror position (15 bins). The model is quadratic in sea surface temperature, but independent of sea surface winds and salinity. The model was created by P. Rozenkranz and is also used in ACRS. The emissivity of the ices are tabulated and depend only on frequency. Microwave reflectivities are not used by the microwave RTA, and are not generated by the AL2SS.

5.2 Infrared Surface Model

The infrared surface model adopts a similar approach to the microwave model in describing the radiative properties of each footprint in terms of the surface material properties. Currently 8 materials are used. These include sea water, 2 types of ices, 2 types of soils and 3 types of vegetation. All materials are assumed to be Lambertian emitters in the infrared.

5.2.1 Surface Composition

The contribution of each material is determined by land fraction, the amount of vegetation, the types of vegetation defined by the International Geosphere Biosphere Programme (IGBP) land use surface classification, and 3 or fewer random uniform normalized variates.. This is based on a method used by the Surface and Atmosphere Radiation Budget group of the CERES project [Wilber *et. al.*, 1999]. The IGBP assigns one of 18 land use classes (listed in Table 5) based on the types of vegetation. The IGBP land use class of each footprint is determined from a digital IGBP land use map shown in Figure 12. The map has longitude

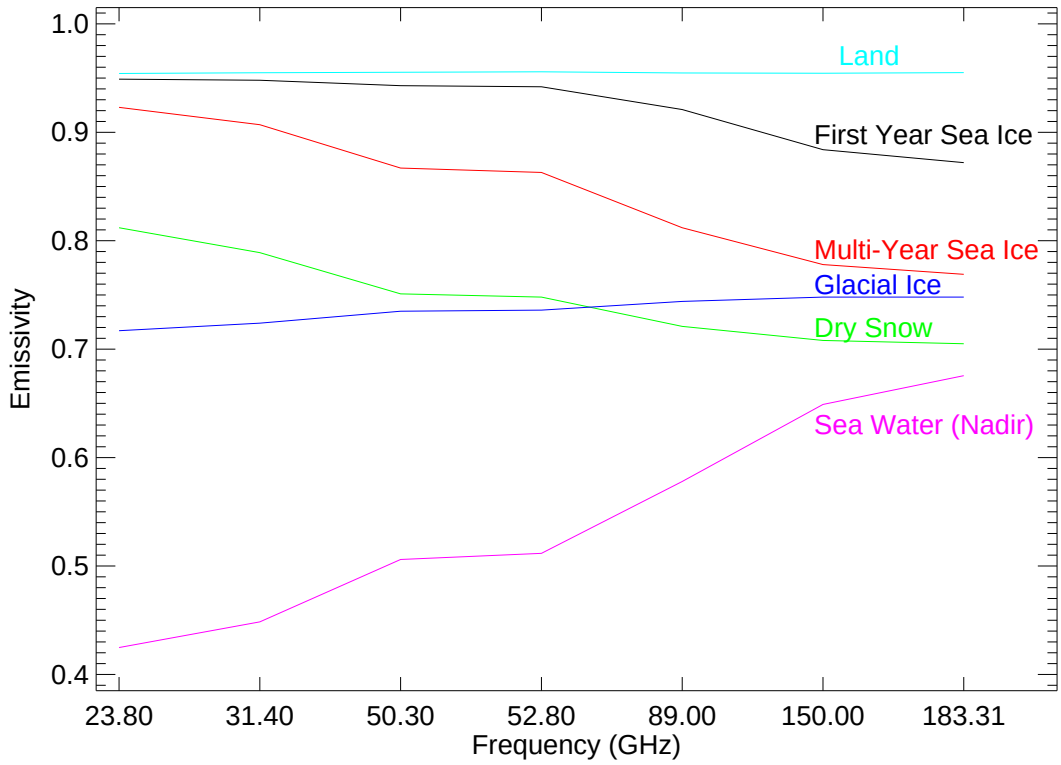

Figure 11: The material emissivity models for land, first year and multi-year sea ice, glacial ice and dry snow and sea water. Sea water is for nadir viewing.

and latitude bins of fixed $10'$ width with the first bin centered on (90° N, 0° E). In the simulations the IGBP land class is determined by the value of the grid box containing the center of an AIRS footprint, rather than the footprint area-weighted average.

The 18 IGBP land use classes are further simplified to 10 IR surface classes using the CERES scheme. The CERES project than assigned emissivity spectra to each spectral class using fixed fractional contributions of the 8 materials (see Table 4 of Wilber *et. al.*, 1999 for details). In the AIRS simulations this approach would not provide enough variability for AL2SS. Therefore the variability was increased using AVHRR imagery and random variates.

Each footprint is composed of dry soil, vegetation and water. Vegetation and water amounts are determined from AVHRR NDVI imagery and the sampled DGM. The largest variability occurs over land from variable vegetation amount. The vegetation fractional coverage, f_v, is derived from a linear relation between vegetation areal coverage and NDVI

$$f_v = \begin{cases} 0 & : \quad \mathrm{NDVI} < 0.1 \\ 2\,\mathrm{NDVI} - 0.2 & : \quad 0.1 \leq \mathrm{NDVI} < 0.6 \\ 1 & : \quad 0.6 \leq \mathrm{NDVI} \end{cases} .$$

The least vegetated sands, correspond to no coverage, has an NDVI of 0.1. The Amazon rain forest, corresponding to total coverage, typically has NDVI values around 0.6 [Lambin and Ehrlich, 1996]

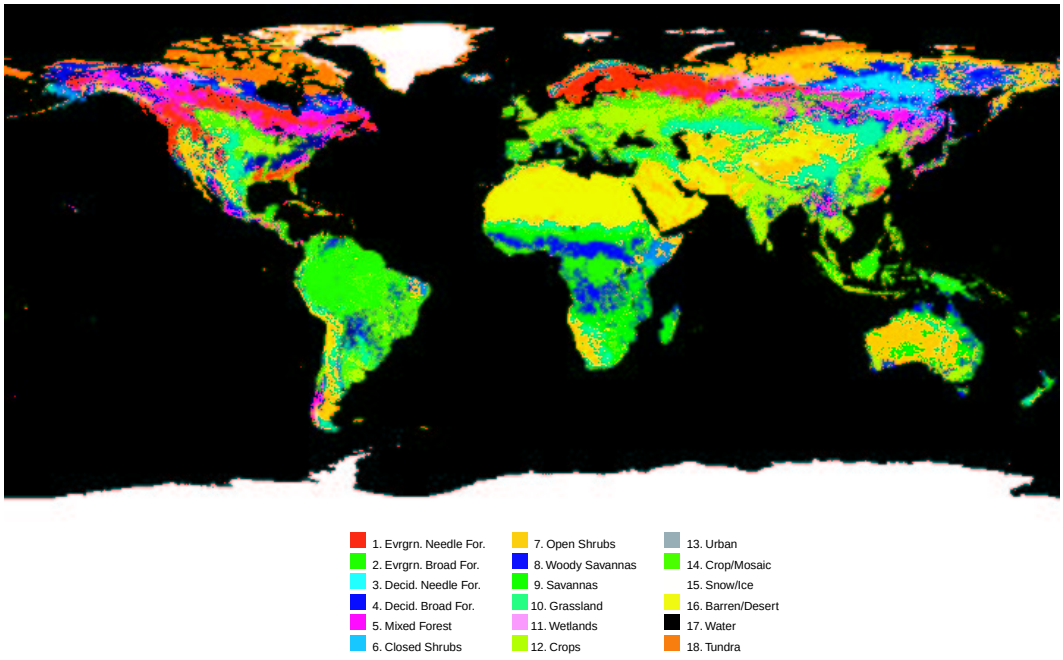

Figure 12: The IGBP land cover usage map, rotated with the prime meridian in the center, color coded by use classification

NDVI is obtained by interpolating the NDVI map to the center position of the footprint. There is no averaging over an AIRS FOV so the value for the footprint is that of the pixel closest to the center. Modelled local variability may be unrealistically large. The derived fraction is the amount of vegetation in the land part of the footprint; the vegetated fraction of the footprint is the vegetation fraction times the land fraction.

Vegetation type is determined from the spectral class and can be either coniferous forest, deciduous forest or grassland. The IR surface class determines the types of vegetation present in the footprint, but not the relative amounts. When two types of vegetation are present, normalized uniform variates α_1 and α_2 determine their relative contributions. The normalization is $\alpha_1 + \alpha_2 = 1$. IR surface class 7 contains 3 types of vegetation and normalized variates β_1, β_2 and β_3 determine their relative contributions; a similar normalization applies.

The composition of the non-vegetated land component is also determined by the spectral class. It can be either quartz sand, water, a mixture of ices either dry or wet and “urban” development. Water is assumed to cover part of the land fraction where the IGBP class is permanent wetland (spectral class 5). In this case, the effective water fraction is increased by the non-vegetated land fraction. Occasionally the IGBP class is water, but the land fraction is nonzero, e.g. near coastlines or small islands. In such cases the spectral class of the geodetically closest non-water footprint in the granule is used. If none exists, IR class 4 is assumed.

The algorithm for determining the fractions is summarized in Table 6. The surface properties file generator determines the fractions and writes them along with IR surface class, NDVI and time to the surface

IGBP Class	Description	IR Surface Class
1	evergreen needleleaf	1
2	evergreen broadleaf	1
3	deciduous needleleaf	2
4	deciduous broadleaf	2
5	mixed forests	3
6	closed shrublands	3
7	open shrubland	3
8	woody savannas	4
9	savannas	4
10	grasslands	4
11	permanent wetlands	5
12	croplands	4
13	urban	6
14	mosaic	7
15	snow/ice	8
16	sparsely vegetated	4
17	water	0
18	tundra	9

Table 5: The 18 IGBP land use classes and the IR surface class assigned to each land use class .

properties file. Infrared emissivities and reflectivities are calculated in the AvnSim file generator.

5.2.2 Emissivity Model

The AvnSim files contain emissivities and reflectivities at 39 hinge point frequencies. The RTA interpolates linearly in frequency to obtain the emissivity or reflectivity at frequencis in the range of the hinge points. The end hinge point values are used outside that range,. The AIRS instrument focal plane has 17 detector modules that can be assigned to 3 spectral regions. The hinge points were selected to cover the AIRS spectral bandpass, and have three groups. Table 7 list the properties of each group of hinge points. It also list the AIRS detector modules covered by the group. The hinge point frequencies are shown in Figure 13. The emissivities are interpolated from tables spanning the range $645\,\mathrm{cm}^{-1}$ to $2670\,\mathrm{cm}^{-1}$ with $5\,\mathrm{cm}^{-1}$ resolution.

The emissivity tables for the ices and vegetation are interpolated from emissivities produced by the CERES group. The CERES values are band-average spectral response functions of the the 12 CERES channels and are derived from the Johns Hopkins University spectral library [Salisbury and D'Aria, 1992]. The CERES tables do not extend to the high end of the AIRS range and have channel centers from $140\,\mathrm{cm}^{-1}$ to $2150\,\mathrm{cm}^{-1}$. The CERES emissivities were interpolated to the table frequencies using cubic spline interpolation within the CERES spectral range. The table was extended at high frequencies using linear extrapolation. The resulting tables are plotted in Figure 13

Spectral Class	Material						
	water	ice/snow	black	quartz	grass	conifer	deciduous
0	1						
1				$1-f_v$		f_v	
2				$1-f_v$			f_v
3				$1-f_v$		$\alpha_1 f_v$	$\alpha_2 f_v$
4				$1-f_v$	f_v		
5	$1-f_v$				f_v		
6			$1-f_v$		f_v		
7				$1-f_v$	$\beta_1 f_v$	$\beta_2 f_v$	$\beta_3 f_v$
8		$1-f_v$				f_v	
9		$1-f_v$			f_v		

Table 6: Algorithm for evaluating the relative component of each material in the land cover fraction of a footprint. The column labeled ice/snow applies to two separate and exclusive ice components; snow for spectral class 8 or wet ice (tundra) for spectral class 9. f_v is the vegetation fraction and α and β refer to random variates described in the text.

First (μm)	Last (μm)	Separation (μm)	Number	AIRS Modules
15.4	8.6	0.2	18	5-12
8.3	6.1	0.2	12	3, 4A-4D
4.6	3.8	0.1	9	1A, 2B, 2A, 1B

Table 7: Summary of infrared hinge points. The hinge points are divided in three groups. For each group the first wavelength, the last wavelength, the spacing between hinge points, the number of hinge points in the group, and the AIRS instrument modules spanned by the group.

Emissivities of the two soil types were obtained from the Infrared Handbook [Wolfe and Zissis, 1978] and a simplified model. The CERES quartz emission table were not used because the strong quartz absorption feature near 1000 cm^{-1} was poorly represented. A higher resolution emission model was provided by Figure 3-98 (electronic scan of page3-92) of the Infrared Handbook. The simple model for urban soil is a perfectly black (emissivity equal to 1) materials such as might be expected from glasses such as asphalt and concrete. Urban soil is found only where the IGBP land use class identifies the location as urban. The quartz emissivity model is shown in Figure 13.

The Masuda sea water emissivity model [Masuda *et. al.*, 1988] is used to determine the emissivity

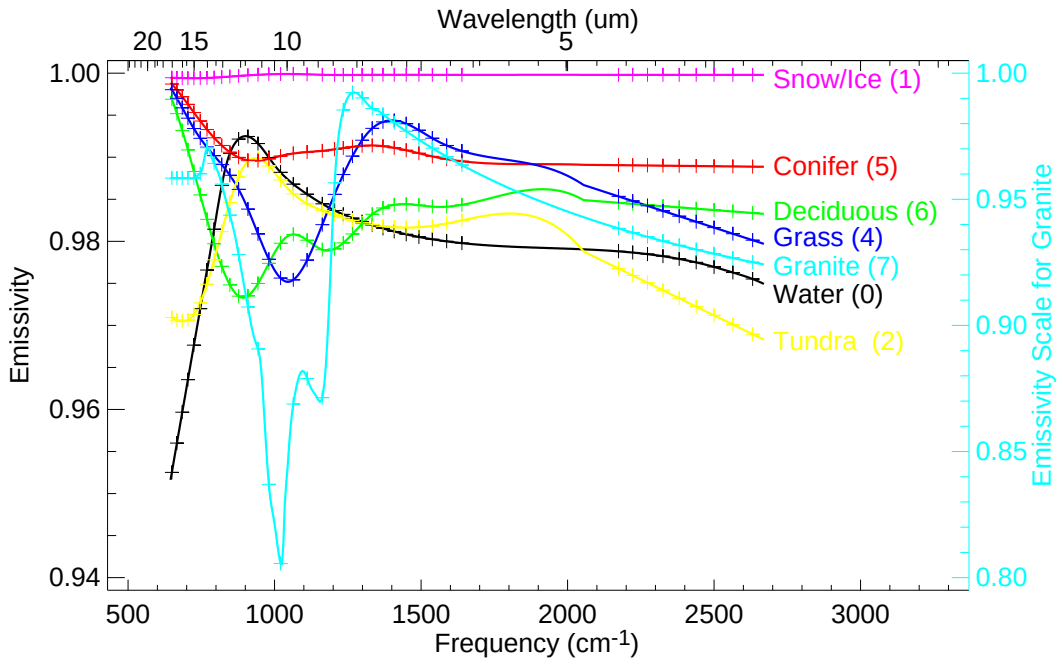

Figure 13: The material emissivity models for (0) sea water (nadir), (1) snow/ice, (2) tundra or wet snow, (4) grass, (5) conifer forest, (6) deciduous forest and (7) granite. The scale on the right side applies to granite. The positions of the emissivity hinge points are show by + symbols.

of sea water. The model depends on frequency, emission angle and wind speed. The original Masuda model is a table of emissivities at the frequencies of the High Resolution Infrared Sounder (HIRS) channels. T.J. Kleepsies at NOAA/NESDIS [documented in software provided by C. Barnet at GSFC] fit an analytic function to the data of the form,

$$\epsilon(\nu,\theta,W) = C_{10} + C_{11}W + C_{12}W^2 + \Big\{(C_{20}-C_{10}) + (C_{21}-C_{11})W + (C_{22}-C_{10})W^2\Big\} \times \exp\left[\frac{(60^\circ - A_3)^2 - (\theta - A_3)^2}{A_0 + A_1 W}\right] ,$$

where arrays A and C are tables of coefficients indexed by HIRS channel (frequency), θ is the emission angle in degrees and W is the wind speed in m/s. The Masuda data spans 769 to 2857 cm^{-1} (3.5 μm). The coefficients are interpolated to cover the spectral interval 645 to 2670 cm^{-1} in 5 cm^{-1} bins. The coefficients are interpolated in frequency using cubic splines within the range of the original Masuda data. Linear extrapolation is applied outside this range. Figure 14 shows some representative IR emissivities plotted against frequency and emission angle for several wind speeds. Emissivity is strongly dependent on emission angle, varying by greater than 5% from 30° to 55°. Emissivity is weakly dependent on frequency above about 800 cm^{-1}.

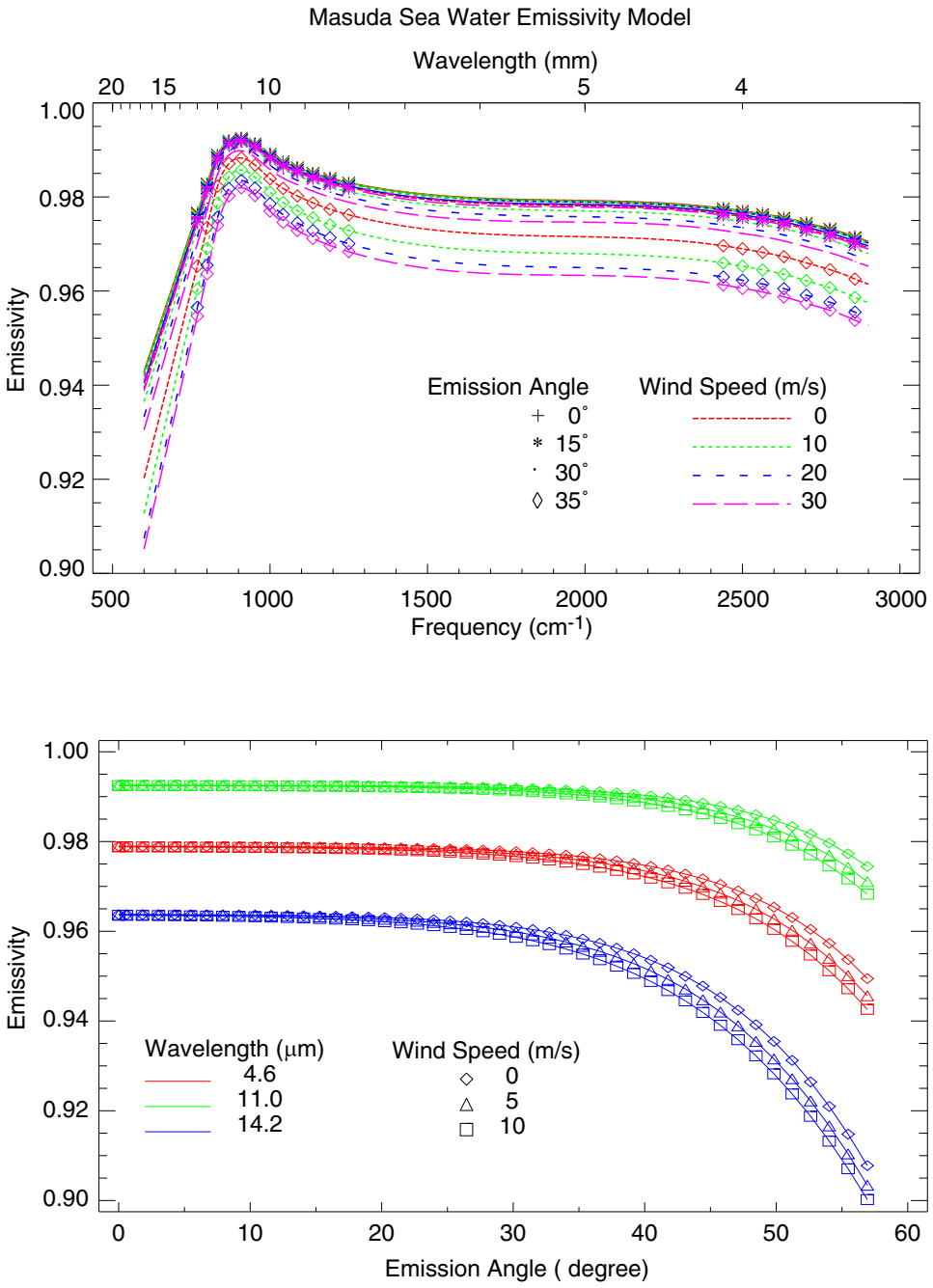

Figure 14: The Masuda sea water emissivity model. The upper panel shows the dependence versus frequency at emission angles of 0° (+), 15° (∗), 30° (line only) and 45°(⋄) and wind speeds of 0 m/s (red), 10 m/s (green), 20 m/s (blue) and 30 m/s (magenta). The symbols show the frequencies of the HIRS channels. The lower panel shows the dependence on emission angle at wavelengths 4.6 μm (red), 11 μm (green) and 14.2 μm (blue) for wind speeds of 0 m/s (⋄), 5 m/s (△) and 10 m/s (□).

6 Cloud Properties

Simulation cloud properties include cloud top and bottom pressures, cloudiness, liquid water amount, and emissivity and reflectivity. A complete list of simulation cloud properties, their units and their location in the AvnSim output file footprint records can be found in Table 14.

The forecast output has three cloud layers referred to as “high”, “mid” and “low”. Each layer has a cloud top pressure, a cloud bottom pressure and a cloudiness (total cloud cover); 0% cloudiness indicates a clear layer. The simulations uses two of these, preferably high and mid layer. Low is use if either of the upper layers have zero cloud amount. Cloud layers within 25 hPa of the surface are never used, however. Figure 15 show the distribution of cloud top pressure for the 15 December 2000 simulation. The clouds

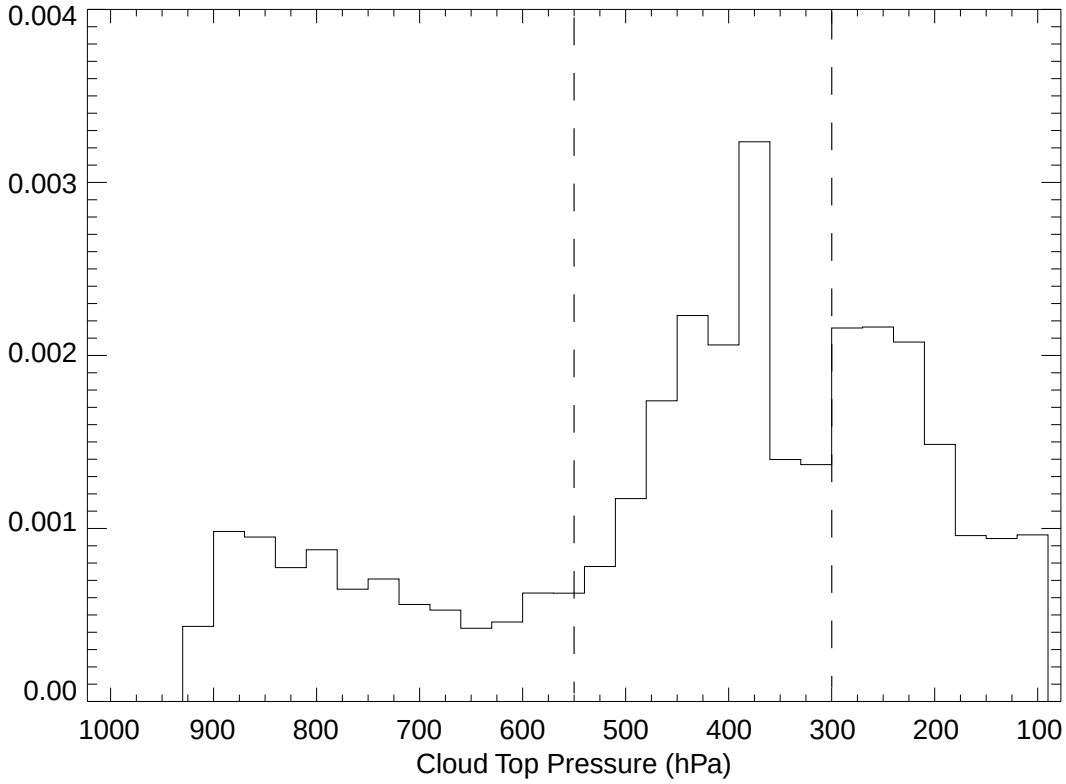

Figure 15: The distribution of cloud top pressures.

divide into three groups with boundaries on cloud top pressure at 550 and 300 hPa. The boundaries are placed symmetrically around the peak of the central group.

Cloud top and bottom pressures are interpolated from the forecast to the location of the footprint using bilinear interpolation in each of the forecast layers. The interpolation may include grid boundaries where cloudiness is zero, and therefore cloud properties such as cloud top and bottom pressure are not defined. The forecast fields transition smoothly into these undefined regions, so the interpolation is well behaved. The interpolations are evaluated independently for each footprint; correlations in cloud properties within the 9 footprints of a retrieval set arise from coarseness of the model. Although any footprint has only two cloud

layers, a retrieval set can contain three.

The forecasted cloudiness are means within a $1^\circ \times 1^\circ$ box. The simulations require cloud variability on the scale of an AIRS footprint, i.e. ≈15 km, or a small fraction of a model grid box. Cloud variablility is modelled by using the interpolated forecast cloudiness as a mean amount and adding a random component. The simulated cloudiness is derived from a normal variate with its mean equal to the interpolated model cloud amount $f^c_{m\,i}$, and its standard deviation σ equal to $0.3 f^c_{m\,i}$. Cloudiness is bounded within the interval [0,1]. The index i is over cloud layer and different random numbers are used for each cloud layer and footprint. The cloudiness is

$$f^c_i = f^c_{m\,i} + 0.3 f^c_{m\,i} n \ ,$$

where n is a random number from a normal distribution and i is an index over cloud layer. The sequence of random number, one per reported cloudiness should be uncorrelated, but this has not been examined. The cloudiness generated by the level 2 PGE and used by the RTA is the viewed cloudiness, i.e. the fraction of the footprint covered by the cloud layer and visible to the instrument. The simulations uses the random small cloud approximation, which assumes that clouds are much smaller than the FOV and cloud positions in the two layers are uncorrelated. The viewed fraction is:

$$f^c_{v\,i} = \begin{cases} f^c_1 \\ (1 - f^c_1) f^c_2 \end{cases} \ .$$

The output file contains both viewed and true cloudiness.

Figure 16 compares maps of forecasted and simulated cloudiness. Simulated cloudiness is the forecasted cloudiness plus a 30% random component bounded in the interval [0, 1]. The simulated field appears unusual at very low or high cloudiness, such as north of western Australia and north of eastern New Guinea. When the forecasted cloudiness is large, the simulated field is highly variable and has a mean much smaller than the forecast. Figure 17 shows how the simulated mean cloudiness departs from the forecast cloudiness when the forecast cloudiness exceeds 0.6. This arises because cloudiness is sampled from an unbounded distribution, but is bounded by [0,1]. At low mean cloudiness, the simulated field appears overly homogeneous.

Figure 18 show maps of simulated cloudiness mean and standard deviation. The mean and standard deviation are evaluated from the nine footprints in each retrieval set and the standard deviation is relative to the mean of that retrieval set; therefore represent cloud variability over 50 km length scales. As discussed above, simulated mean cloudiness agrees with the forecast cloudiness when it is less than 0.6. It is less variable and it is never larger than 0.8 (see north of eastern New Guinea). Similarly standard deviation is small whenever the mean cloudiness is small, but never when the cloudiness is large. This implies that some meteorological conditions are not represented in the simulations. One such condition is uniform clouds extending across several retrieval sets (mean cloudiness near 1 and standard deviation near 0). Isolated cloud systems such as equatorial cumulus systems where clouds a few kilometers across are often tens of kilometers apart (mean cloudiness near zero and standard deviation between 0 and 0.25) are also not represented in the simulations.

Cloud liquid water or ice has a fixed density $\rho_{lw,i} = 0.3 \times 10^{-3}$ kg/m^3 for clouds below 500 hPa and 0.03×10^{-3} kg/m^3 for clouds above 500 hPa. Clouds are composed of ice (the cloud ice flag `ciw` is set to 1) when the ambient air temperature is less than or equal to 245 K. A survey of cloud particle sizes, and liquid water or ice densities can be found in Borovikov *et. al.* [1963]. AIRS Science Team Design File Memo, ASDF-006-1995- MDH [available from M. Hofstadter, JPL] describes the selection of cloud properties for use in the Level 1B visible simulations. The average water density over a footprint is the cloud density multiplied by cloudiness f^c_i. The layer amount is the cloud density multiplied by the fraction of the layer thickness contained in the cloud. The nature of the liquid water simulations changed dramatically in

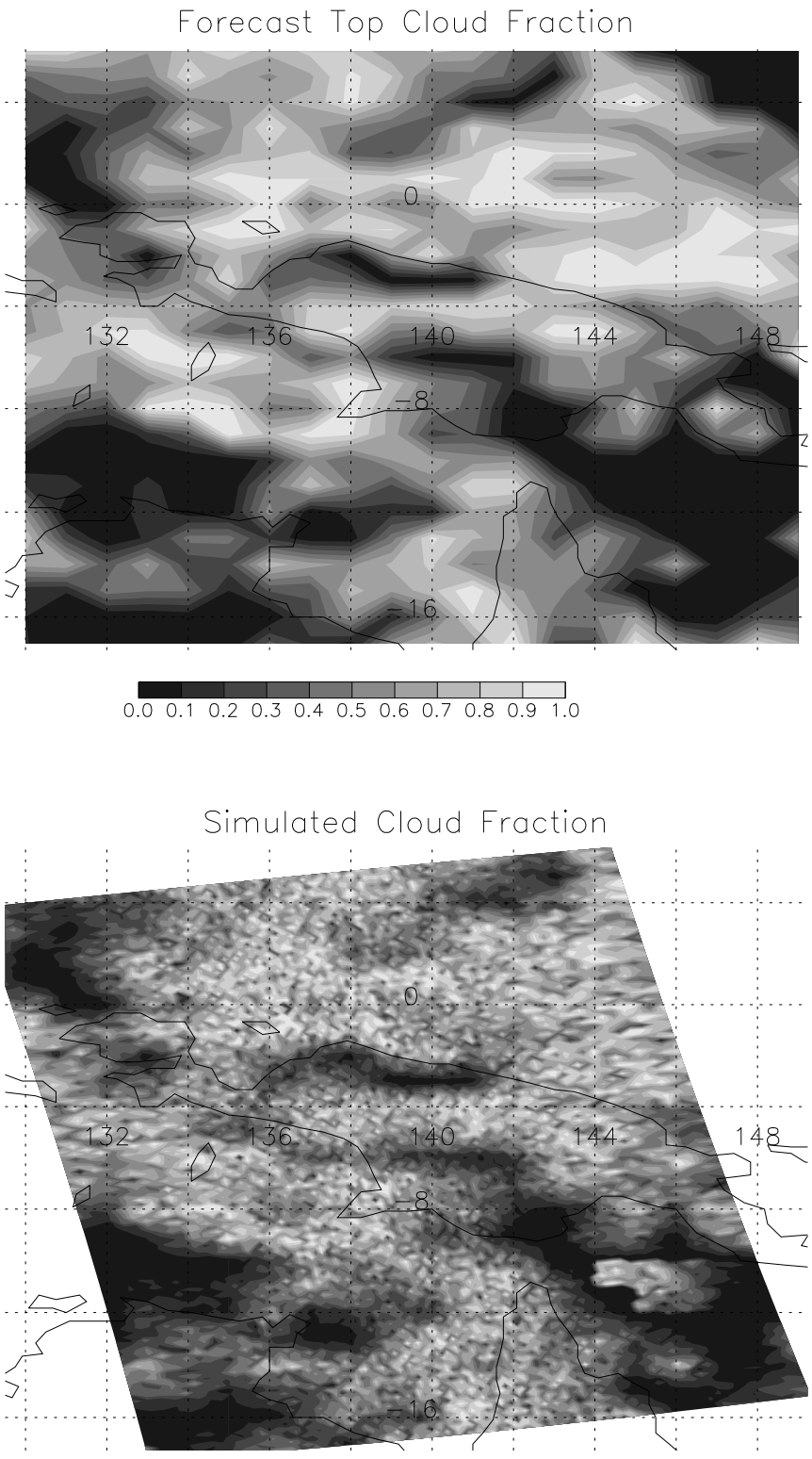

Figure 16: Upper level cloudiness for Granule 42 on 15 December 2000. The upper panel shows the forecasted cloudiness from the 3 hour forecast of the 00 UT run; the lower panel is the simulated cloudiness.

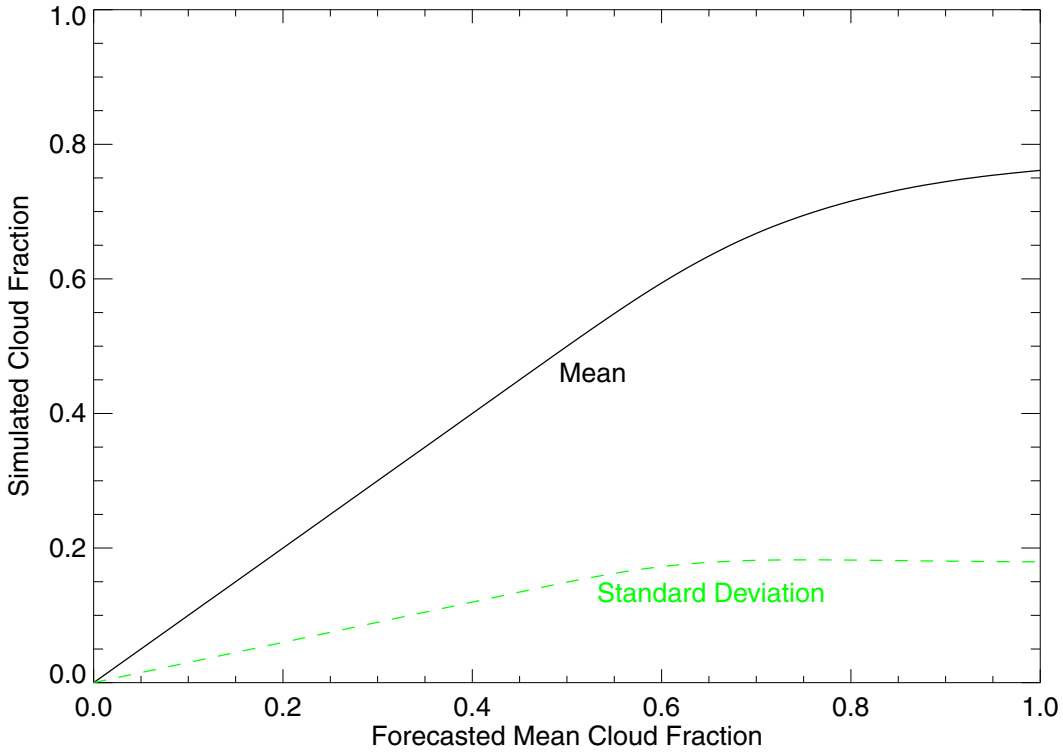

Figure 17: The dependence of the simulation cloudiness mean and simulation cloudiness standard deviation on forecast cloudiness.

February 2001. Prior to February 2001 the conversion to layer amount was performed on the forecast grid, layer amount was not scaled by the fraction of the layer contained in the cloud, and was set to zero if the bottom of the layer was not contained in the cloud or was at a pressure less than 500 hPa. These algorithmic changes resulted in dramatic changes, both increasing and decreasing the resulting liquid water profiles.

Clouds are assumed to be opaque and Lambertian. Cloud emissivity and reflectivity is assumed to vary linearly between specified hinge points, as is the case for surface properties. All cloud radiative properties use the 5 spectral hinge points listed in Table 8. The emissivities are random and are sampled from a normal variate with mean of 0.9 and σ of 0.01. Cloud emissivities are bounded between 0.5 and 0.99 and uncorrelated in frequency. A new sequence of emissivities is generated for each layer and each footprint. Therefore, the random component of the emissivity is uncorrelated between the 9 footprints in a retrieval set.

7 Local Variability

One of the greatest challenges in the simulation is adding realistic variability at spatial scales of or finer than the AIRS FOVs. Global meteorological data sets are inherently smooth at the roughly 15 km-scale AIRS sampling because typical models have horizontal resolution of 1°or greater. This is acceptable in the case of most profile fields as discussed below. Modeled infrared surface properties have the AVHRR 1 km

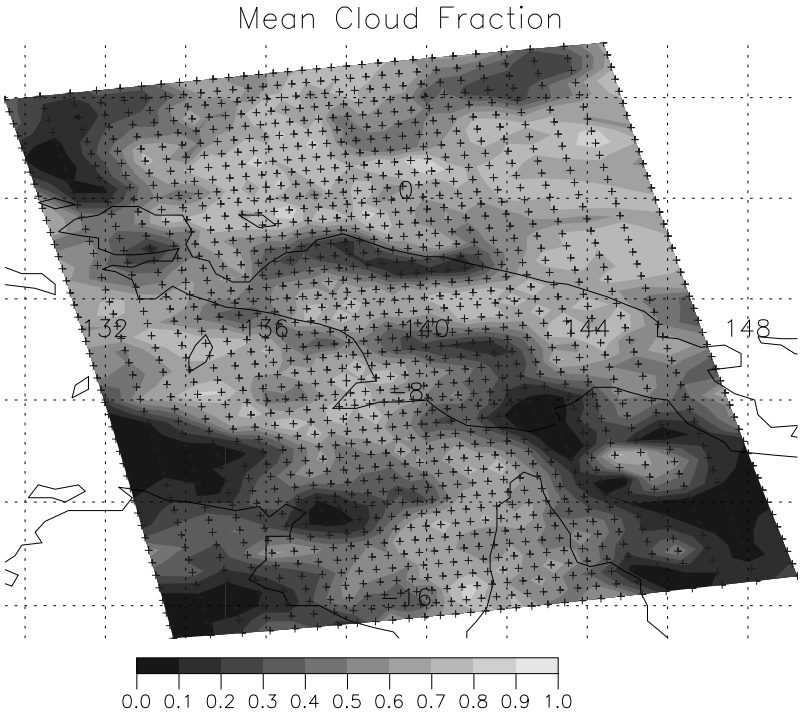

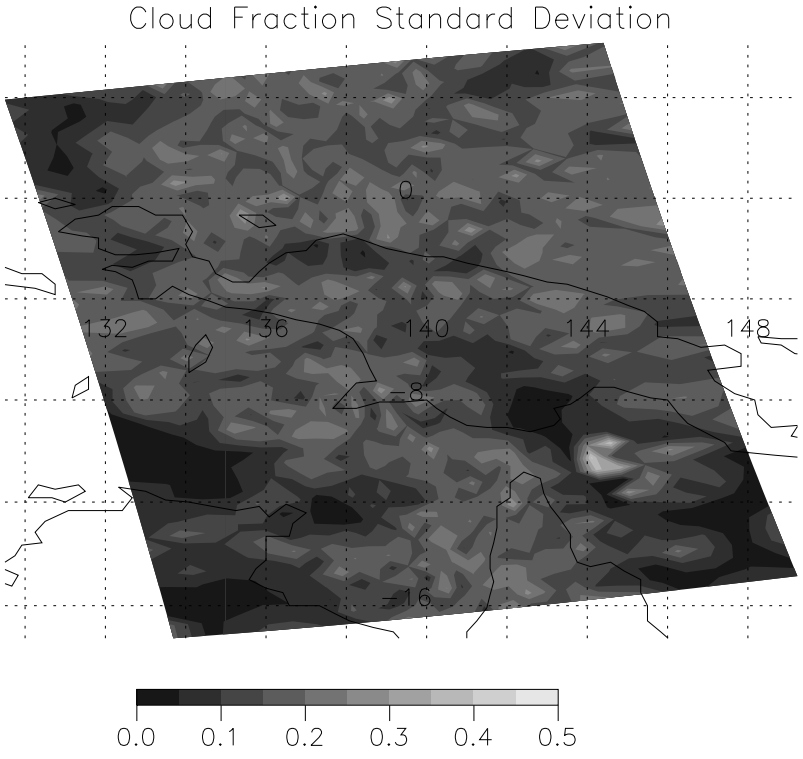

Figure 18: The mean cloudiness (upper panel) and standard deviation (lower panel) within retrieval sets for Granule 42 of the 15 December 2000 simulations.

Frequency (cm^{-1})	660	909	1111	2105	2700
Wavelength (μm)	15.15	11	9	4.75	3.7

Table 8: Cloud infrared hinge points.

image resolution, as discussed above, while other fields have random variability added at the scale of AIRS footprints. This section describes the amount of local variability in example fields. All figures are derived from an analysis of the 15 December 2000 simulation, decimation to the first scanset of each granule.

Local variability can be characterized by the difference between a parameter and its mean value within a retrieval set

$$\delta X_{i,j} = Xi, j - \bar{X}_i$$

We refer to this as the "local difference". The parameter X is any geolocated parameter, the first subscript indicates retrieval set and the second index indicates footprint within the retrieval set. The mean of parameter X for retrieval set i, referred to as the "local mean" is

$$\bar{X}_i = {}^1\!/_{N_i} \sum_{j=1}^{9} X_{i,j}$$

where N_i is the number of footprints in retrieval set i. Nominally N_i is 9 except when some of the footprints have missing data. This commonly occurs for some cloud parameters which are undefined when the cloud fraction is 0. Means and standard deviations evaluated from global data sets are referred to as "global".

Figure 19 shows a histogram of local differences of surface temperature. The data set is global and contains 9 local differences from 7200 retrieval sets. We desire a statistic which describes the amount of local variability in a global data set. The surface temperature distribution is approximately normal, but a χ^2 test indicates that the data contains more outliers than are expected. This suggests that local variability can be described by statistics which include the local standard deviation

$$\sigma_{\delta X} = \left\{ \frac{1}{\mathbf{N} - M} \sum_{i=1}^{M} \sum_{j=1}^{N_i} \delta X_i^2{}_{,j} \right\}^{1/2} ,$$

the maximum absolute local difference

$$\delta X_{\mathrm{Max}} = \max \delta X \ ,$$

or the center-derived local standard deviation

$$\sigma'_{\delta X} = \frac{\delta X_{\frac{1+\alpha}{2}\mathbf{N}} - \delta X_{1+\frac{1-\alpha}{2}\mathbf{N}}}{2^{3/2}\ \mathrm{erf}^{-1}(\alpha)}$$

The center-derived local standard deviation is derived from a sample of δX around the median; a single index on δX indicates an ordering from smallest to largest, and α is the fraction of local differences used, normally around 0.5. The number of differences is $\mathbf{N} = \sum_{i=1}^{M} N_i$. Our studies have shown that $\sigma_{\delta X}$ and $\sigma'_{\delta X}$ give approximately the same number for the simulations, consistent with the χ^2 analysis.

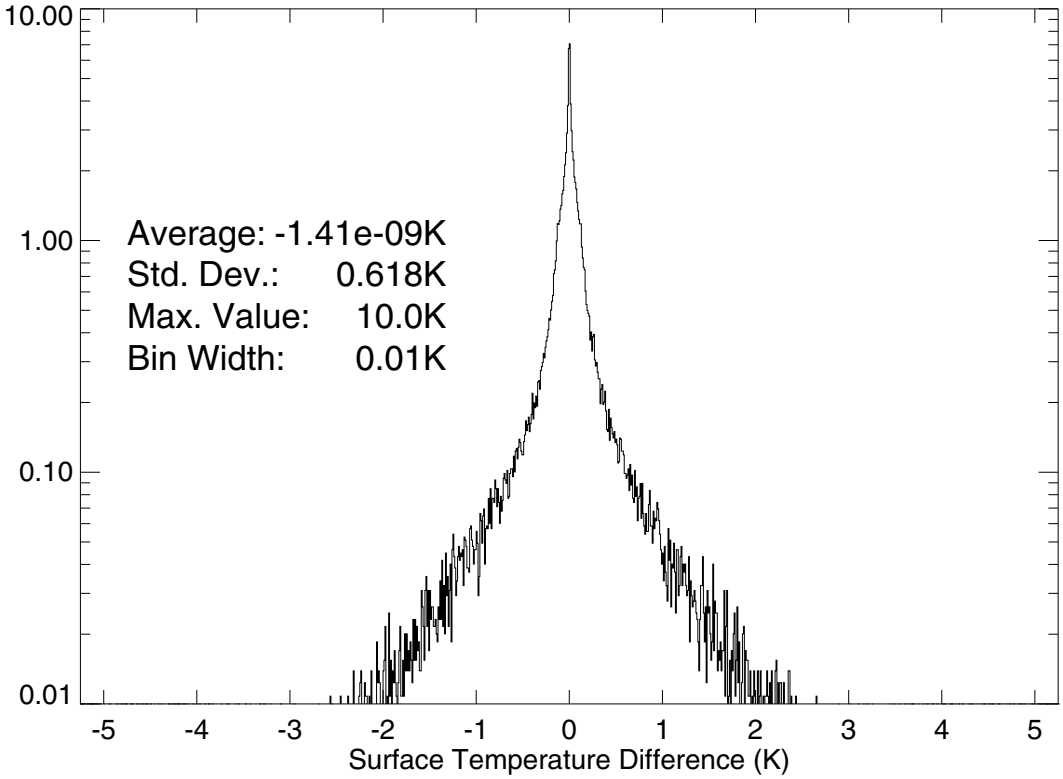

Figure 19: Distribution of difference between surface skin temperature and retrieval set mean surface temperature for decimated 15 December 2000 simulations.

The simulated temperature and H_2O fields are interpolated from the forecast (plus climatologies) without the addition of random variability. Figures 20 and 21 show the local standard deviations and maximum differences of temperature and water vapor. The global standard deviation characterizes the variability AIRS is designed to observe. The local standard deviation normalized by the global standard deviation characterizes the fraction of global variation present with retrieval sets. This is referred to as the "normalized local standard deviation". The maximum differences normalized by the global standard deviation characterizes local variability in the worse case; this is the "normalized maximum local difference".

Water vapor shows even greater local variability, typically 10% of the global standard deviation and equal to it in extreme cases. Although atmospheric water vapor variability occurs on scales much smaller than the resolution of the forecast model (the bulk of the model moisture cycle is parameterized), water vapor is still highly variable in the model fields.

Ozone local variability is shown in Figure 22. The ozone simulation uses the UARS zonal-mean monthly climatology above 10 hpa, forecast model fields between 100 hPa and 10 hPa, and the tropospheric climatology with its $4^\circ \times 5^\circ$ horizontal resolution below 100 hpa. The normalized local standard deviation for ozone is similar to temperature in the troposphere and is around 0.1, but can be greater than 1 in extreme cases. Surprisingly, the forecast model ozone has less local variability than the climatology. In summary, local variability in the profile quantities of temperature, water vapor and ozone have considerable local variability

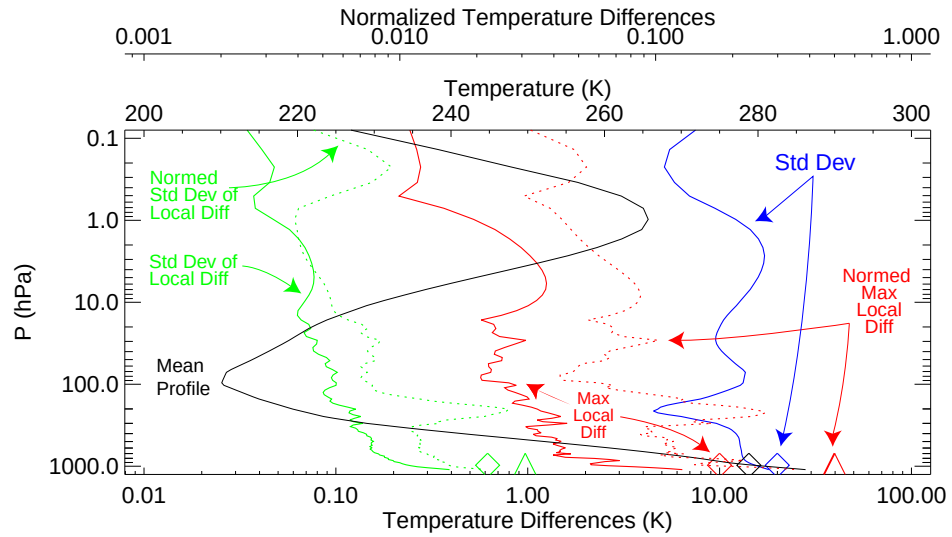

Figure 20: Temperature local variability. The mean profile and global standard deviation are shown by the black and blue curves. The local standard deviation, the maximum local difference are shown by the solid green and red curves. The normalized local standard deviation and the normalized local maximum difference are shown by the dotted green and red curves. The lower axis applies to the difference curves, the scale above the plot applies to the mean profile, and the uppermost scale applies to normalized differences. Skin temperature and its differences are shown by diamonds; normalized differences by triangles. Surface skin temperature is plotted at the mean surface pressure, 972 hPa.

without any attempt to model it with added random samples.

Some of the largest variability can be found in surface properties. Scalar parameters of elevation, land fraction, surface pressure and surface skin temperature are sumarized in Table 9. Some of the largest normalized variability occurs in fields derived from the DGM: elevation, land fraction and surface pressure (the largest component of surface pressure variability is the elevation correction applied to the sea level pressure). Water vapor burden has a maximum normalized local difference comparable to the DGM derived fields.

The local variability of surface microwave emissivity, infrared emissivity and infrared reflectivity are shown in Figures 23, 24 and 25. Microwave emissivity is from a model constant over pure ocean or ice, slightly random over sea ice, and random over land. The random component produces 20% local variability, but the local variability can be as large as 3 times the global variability near coastlines and the edges of ice boundaries. The normalized local variability of infrared and microwave emissivity have similar ranges: a maximum of 3 to 4 and a normalized local standard deviation around 0.3. This is in contrast to the microwave and infrared global standard deviations which are 0.1 to 0.2, and 0.01 to 0.05. respectively. The infrared surface emissivity, and all statistics derived from it, show the quartz absorption band between 800 and 1200 cm^{-1}. This band is the largest source of emissivity variability, via variability in land fraction and vegetation cover. The largest local emissivity differences can be larger than 0.15 and are associated with retrieval sets containing both ocean and desert footprints. The corresponding brightness temperature difference at 300 K is about 10 K. The frequency dependence of infrared surface reflectivity has greater

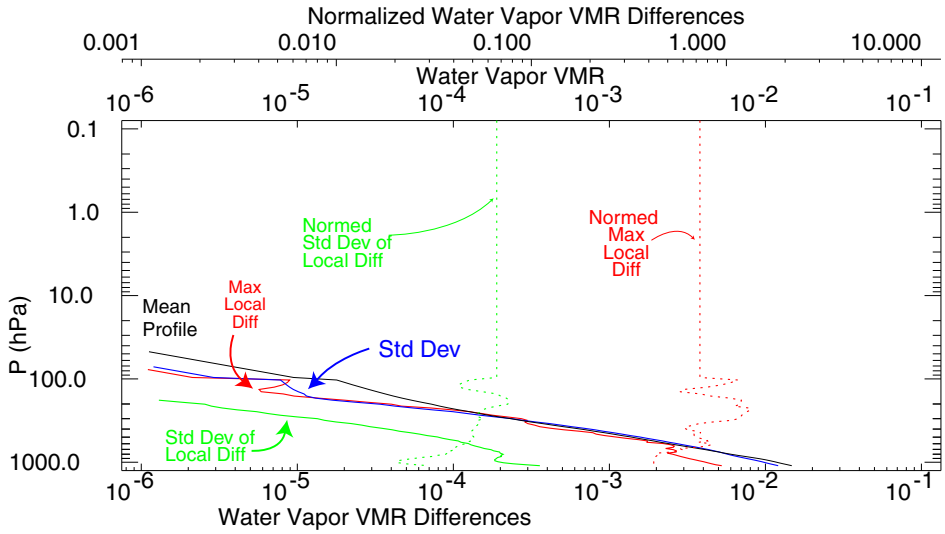

Figure 21: Statistical assessments of H_2O vapor profiles as described in Figure 20

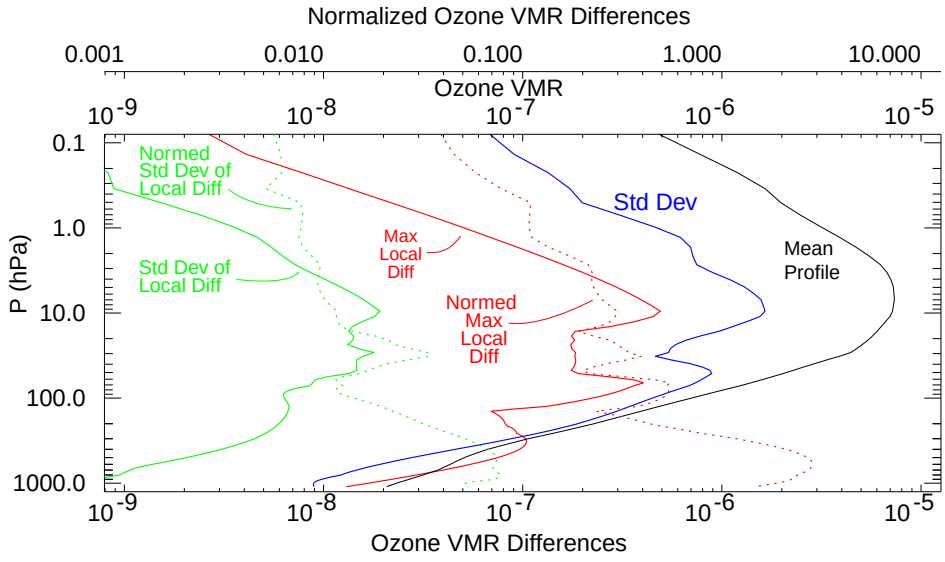

Figure 22: Statistical assessments of O_3 profiles as described in Figure 20

variability simply because small changes in emissivity cause large relative changes in reflectivity when the emissivity is close to one. The normalized local variability of emissivity and reflectance are equivalent because all surfaces are Lambertian reflectors.

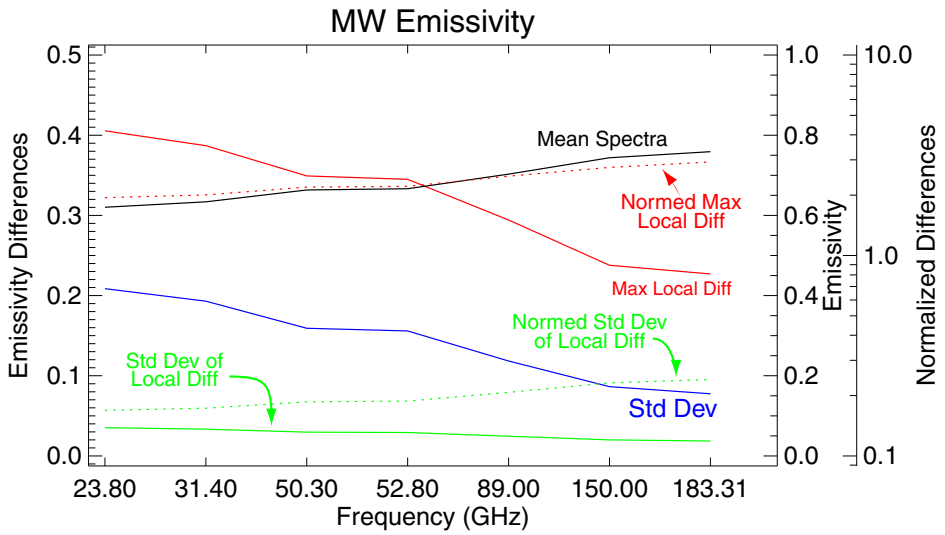

Figure 23: Globally averaged microwave surface emissivity at the hinge points, its local and global standard deviation, the maximum local difference, and the normalized local standard deviation and maximum difference. Colors and line styles are the same as Figure 20. The left axis applies to the local differences and global standard deviation, the innermost right axis applies to the mean spectra and the outer left axis applies to the normalized local differences.

Field	Average	Global σ	$\sigma_{\delta X}$	Maximum δX	Normalized $\sigma_{\delta X}$	Normalized Max. δX
Elevation (m)	339.8	787.5	83.3	1982.6	0.11	2.5
Land fraction	0.33	0.46	0.076	0.8	0.17	1.8
Pressure (hPa)	971.7	86.3	8.99	203.0	0.10	2.4
Temperature (K)	278.8	20.0	0.62	10.0	0.03	0.5
CO_2 (ppmv)	365.2	0.2	0.004	0.16	0.02	0.8
H_2O Burden (mm)	19.1	17.3	0.64	23.4	0.04	1.4

Table 9: Surface property variability (scalar fields) Shown are the global mean value, the global standard deviation, the RMS local difference, the maximum local difference, the RMS local difference normalized by the global standard deviation, and the maximum local difference normalized by the global standard deviation.

Cloud parameter variability comes from the forecast model and added random variates. Cloud parameters are grouped into upper, middle and lower levels using cloud top pressure thresholds at 300 and 550 hPa (see Figure 15 for cloud top pressure distribution and position of boundaries). The statistics defined at the

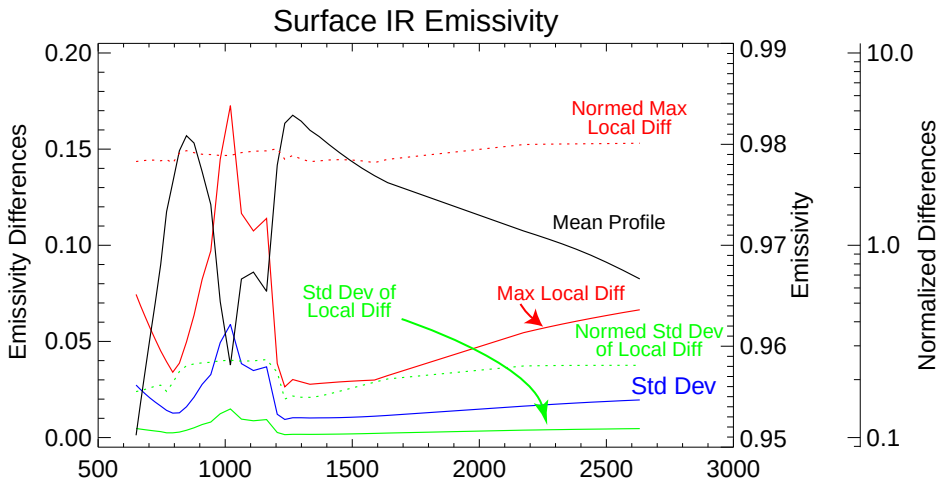

Figure 24: Spectra of the mean infrared surface emissivity and statistics of global and local variability are shown. Colors and line styles are the same as Figure 20

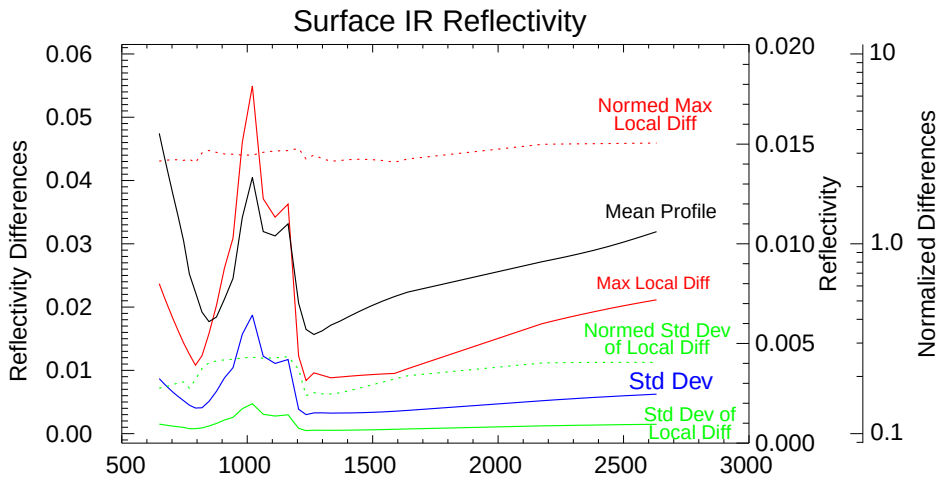

Figure 25: Spectra of infrared surface reflectivity variability as in Figure 24.

beginning of this section are evaluated for cloud top temperature, cloud top pressure and cloudiness within each group. Cloud top pressure and cloud top temperature obtain their local variability exclusively from the forecast, while cloudiness has an imposed 30% local variability. Not surprisingly, normalized cloud top temperature variability is approximately four times smaller than cloudiness variability. Cloud top pressure normalized variability is only a factor of two smaller than cloudiness normalized variability. The larger normalized variability in cloud top pressure is a consequence of the mechanisms which are drive cloud for-

mation and tie cloud top temperature to the logarithm of cloud top pressure. Cloud top temperature and cloudiness have a much greater impact on the radiative state of the atmosphere and we are not concerned that the simulated clouds have large normalized local variability.

Layer	Field Name	Average	Global σ	$\sigma_{\delta X}$	Maximum δX	Norm. $\sigma_{\delta X}$	Norm. Max. δX
Upper	Pressure (hPa)	770	98.7	19.5	289.8	0.197	2.935
	Temperature (K)	271	14.3	1.1	18.7	0.080	1.308
	Fraction	0.090	0.187	0.069	0.763	0.369	4.071
Middle	Pressure	423	55.3	11.4	215.8	0.207	3.902
	Temperature	241	11.9	1.1	23.1	0.096	1.939
	Fraction	0.128	0.197	0.079	0.739	0.401	3.744
Lower	Pressure	214	57.0	4.1	83.4	0.072	1.463
	Temperature	212	9.0	0.9	22.4	0.098	2.476
	Fraction	0.200	0.288	0.093	0.819	0.321	2.839

Table 10: Variability by cloud layer of cloud top pressure, cloud top temperature and cloudiness. See Table 9 for descriptions of statistics.

Cloud emissivity is derived from a random normal variate bounded on the interval [0, 1]. The mean is 0.9 with a standard deviation of 0.01; emissivity is highly correlated in frequency and position. Figures 26 and 27 show the frequency dependence of statistical properties of emissivity and reflectivity. Local differences are evaluated separately for each cloud layer, but the statistics are derived from both layers combined. The local and global standard deviations are equal because the models are independent of retrieval set. The normalized local standard deviation is therefore equal to one. This means that clouds from within a retrieval set will be as spectrally different as clouds from opposite ends of the earth. All clouds are approximately gray; emissivities are approximately equal emissivities.

8 Summary

This report describes data sources, data flow, algorithms and data products of AL2SS. The AIRS, AMSU and HSB measurements depend on a large assortment of geophysical parameters. AL2SS has evolved to become more realistic as more data sources have been added. It produces atmospheric profiles, and surface and cloud properties based on a complicated set of models, consistent with AIRS geolocation information. As the AIRS investigation moves towards validation and error characterization, AL2SS will continue evolving to have greater realism. This will certainly require additional data sources and more refined models. Additionally AL2SS will need to be validated as its requirements change from an algorithm development tool to a one of validation and error characterization. This documents does not address these issues.

We believe global variability in the lower troposphere is suitable addressed with the current system. Global variability in the upper troposphere and stratosphere, local variability everywhere, surface radiative properties, and cloud models need validation and possibly some refinement. In its current state AL2SS is ready for the early phases of validation.

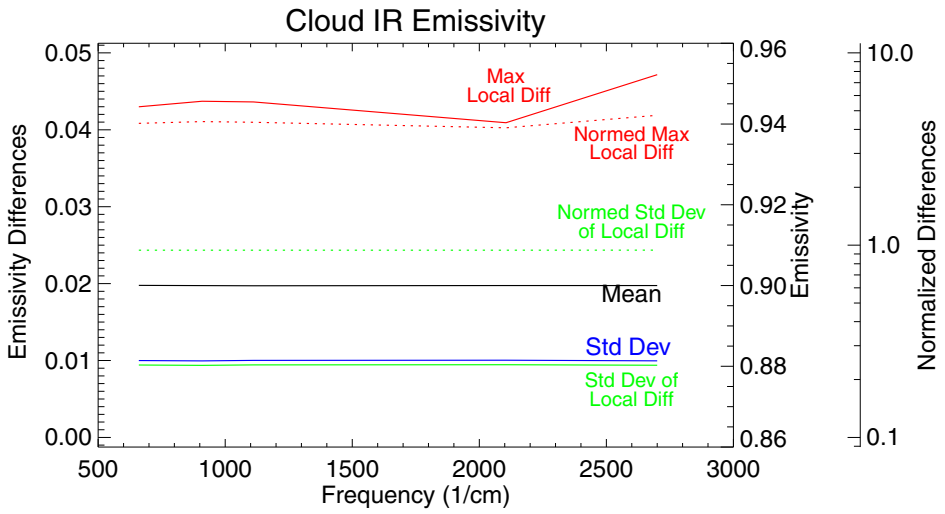

Figure 26: Spectra of the mean infrared cloud emissivity and of global and local variability. Differences are calculated within each cloud layer, but statistics are evaluated from all layers combined. Line styles and colors are the same as Figure 20.

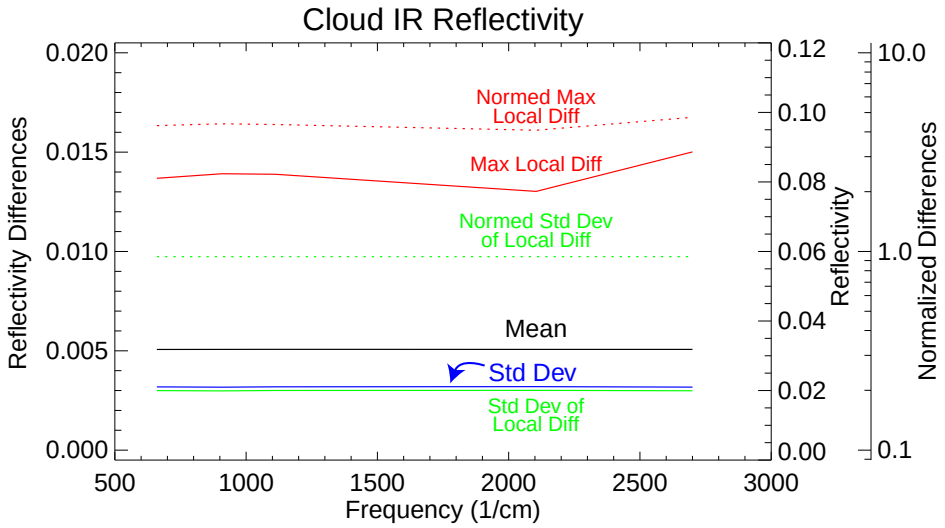

Figure 27: Spectra of infrared cloud reflectivity variability. Same as Figure 26 except for reflectivity.

References

Borovikov, A.M., I.I. Gaivoronskii, E.G. Zak, V.V. Kostarev, I.P. Mazin, V.E. Minervin, A. Kh. Khragian, and S.M. Simeter, *Cloud Physics*, Israel Program for Scientific Translation, 1963.

Derrien, M., *Effect of Cloud Contamination on IASI Spatial Sampling,* Meteo. France Tech. Rep. IA-TN-0000-7615-DIV, 16pp., 1995.

Dey, C.H., *The WMO Format for the Storage of Weather Product Information and the Exchange of Weather Product Messages in Gridded Binary Form as Used by NCEP Central Pperations*, NCEP Office Note 388, 106pp., 1998.

Eidenshink, J.C., and Faundeen, J.L., *The 1km AVHRR Global Land Data Set - 1st Stages in Implementation*, Intl. J. Remote Sensing, 15, 3443–3462, 1994.

Gunson M.R., C.B. Farmer, R.H. Norton, R. Zander, C.P. Rinsland, J.H. Shaw, B.C. Gao, *Measurements of CH_4, N_2O, CO, H_2O, and O_3 in the middle atmosphere by the atmospheric trace molecule spectroscopy experiment on spacelab-3*, J Geophys. Res., 95, 13,867–13,882, 1990.

Lambin, E.F. and D. Ehrlich, *The surface temperature-vegetation index space for land cover and land-cover change analysis*, Intl. J. Remote Sens., 17, 463–487, 1996.

List, R.J., *Smithsonian Meteorological Tables*, Smithsonian Institution Press, Washington DC, 527 pp, 1958.

Logan, J.A., *An analysis of ozonesonde data for the troposphere: Recommendations for testing 3-D models, and development of a gridded climatology for tropospheric ozone*, J. Geophys. Res., 104, 16,115–16,149, 1998.

Masuda, K., T. Takashima, and Y. Takayama, *Emissivity of Pure and Sea Waters for the Model Sea Surface in the Infrared Window Region*, Remote Sensing of the Environ., 24, 313–329, 1988.

Noerdlinger, P.D., *Theoretical Basis of the SDP Toolkit Geolocation Package for the ECS Project*, Hughes Appl. Info. Sys. Tech. Pap. 445-TP-002-002, 201pp., May 1995.

Salisbury, J.W. and D.M. D'Aria, *Emissivity of terrestrial materials in the 8-14μm atmospheric window*, Remote Sensing of the Environ., 42, 157–165, 1992.

Wilber, C.W., D.P. Kratz, S.K. Gupta, *Surface Emissivity Maps for Use in Satellite Retrievals of Longwave Radiation*, NASA Tech. Rep. TP-19999209362, 27pp./ 1999.

Wolfe, W.L. and G.J. Zissis, *The Infrared Handbook*, Office of Naval Research, Dept. of the Navy, Washington, DC, 1978.

A AvnSim File Format

The simulation Level 2 files (AvnSim) contain a complete granule of footprints. Each file is arranged as 45 scansets of 30 retrieval sets, each retrieval set is composed of 9 states, arranged in a 3x3 grid. The files are composed of fixed length records of 4564 bytes, with the first record of the file containing granule attribute. The data is native Sun Microcomputer binary, floating point numbers are IEEE format, integers are signed, and the most significant byte appear first, i.e. big-endian. A sample FORTRAN dump program, "dump_l2_sim.F", and IDL subroutine reader, "read_avnsim.pro", are available.

A.1 Granule Header Record

The granule header record contains granule-specific attributes normally contained in meta-data, or in the HDF attributes, or HDF fields which occur once per file (granule). The granule header also contains dimensioning information making the file self describing. The name and a brief description of each field is listed in Table 11. The type of parameter, length and offset in the record is also given.

A.2 Footprint Data Record

The footprint data records contain 45 fields, which have been divided into four categories, geolocation and data quality, atmospheric profiles, cloud properties and surface properties. These are listed and described in Tables 12, 13, 14, and 15. Generally parameters names correspond to fields in the l2d structure defined in the AIRS Level 2 PGE. However, Some parameters do not have unique structure fields and are placed in integer and real arrays refer to as "ispare" and rspare. When this occurs, the tables below contain a comment indicating in which spare array and at what location.

Name	Description (Units)	Nominal Value	Dim.	Offset
Record_Length	Record length in bytes	4564	I4	0
File_Version	Version of AvnSim File	L2V3A	C5	4
Nobs	Number of Footprint or observations in file	12150	I4	9
Maxemis	Maximum number of IR surface property hinge pts.	100	I4	13
Mxcemis	Maximum number of IR cloud property hinge pts.	7	I4	17
MaxLev	Maximum number of pressure levels	100	I4	21
Maxcld	Maximum number of cloud layers	2	I4	25
Pobs	Pressure of levels top to bottom (hPa)		100R4	29
MwHingeSurf	Maximum number of MW emissivity hinge pts.	7	I4	429
Maxspare	Maximum of real and integer spares	30	I4	433
Typeinst	Instrument associated with footprint pattern	AIRS	C24	437
Granule_Number	Number of granule within dat (1 ... 240)		I4	461
Granule_Size	Number of scansets in granule	45	I4	465
Start_Year	Year in which granule started, (e.g. 2000)		I4	469
Start_Month	Month in which granule started	1-12	I4	473
Start_Day	Day of month in which granule started	1-31	I4	477
Start_Hour	Hour of day in which granule started	1-24	I4	481
Start_Minute	Minute of hour in which granule started	1-60	I4	485
Start_Sec	Second of hour in which granule started	1-60	I4	489
Start_Time	Time at which granule started (secTAI93)		R8	493
Start_Lat	Latitude of spacecraft at start of granule		R8	501
Start_Lon	Longitude of spacecraft at start of granule		R8	509
End_Time	Time at which granule ended (secTAI93)		R8	517
End_Lat	Latitude of spacecraft at end of granule		R8	525
End_Lon	Longitude of spacecraft at end of granule		R8	533
Start_Orbit_Num	Number of Orbit since initialization of Orbit Elements (or Launch)		I4	541
DayNightFlag	String denoting granule local time, (“Day”, “Night”, or “Both”)		C8	545
Node_Type	String denoting orbit section of granule (“Ascending”, “Descending”, “NorthPole” or “SouthPole”)		C8	569
Eq_X_Tai	Nearest time when satellite crosses equator on a descending node (secTAI93)		R8	593
Eq_X_Longitude	Longitude of satellite at EQ_X_TAI (°)		R8	601
Format_Version	Version of AvnSim file	V3A Golf-ball Sim	C24	605
Retrieval_Version	Version of Simulation code	V2.1 AVN Simulations	C24	629
Num_Invalid	Number of invalid footprints in the file	0	I4	653

Table 11: The AvnSim header record contains 33 fields. The units are indicated in the description; secTAI93 are a standard of time defined in section 2.1. Nominal values, are either the range, or the value under all or most conditions. The dimension is a type (’I’ for integer value, ’C’ for character string and ’R’ for floating point) followed by an integer field length in bytes and preceded by an integer repetition count, e.g. 100R4 is an array of 100 4 byte reals.

Name	Description (Units)	Dim.	Offset
Prof ID	A unique ID for each footprint in a granule	C8	0
Lat	Latitude at center of footprint (°)	R8	8
Lone	Latitude at center of footprint (°)	R8	16
TAI Time	Time in seconds since 0000 UT 1 Jan. 1993	R8	24
Sat Zen	Angle from nadir to satellite at the center of footprint (°)	R4	32
Sat Azim	Angle from north to satellite in horizontal at center of footprint (°)	R4	36
Sat Height	Height of satellite from sea level (m)	R4	48
Solar Zen	Angle from nadir to sun at the center of footprint (°)	R4	40
Solar Azim	Angle from north to sun in horizontal at center of footprint (°)	R4	44
AMSU Footprint	Number of AMSU footprint (retrieval set) associated with footprint (0-29)	R4	133
Invalid Flag	A flag set to 1 when a footprint is bad, 0 otherwise	I1	143
View Angle	Angle of scan mirror in rotation dir. relative to instrument nadir (°)	R4	137
Node Type	The orbit segment type of the scan line, either 'A', 'D', 'N' or 'S' for ascending, descending, north pole crossing or south pole crossing, repeated for each footprint, stored in ispare(1)	I4	4324

Table 12: Geolocation, pointing and solar parameters generated by GeoSim process. Columns are as described in Table 11, except nominal values are not relevant. The Profile ID labels the footprint by the scan line number (1-135) and footprint number (1-90), e.g. L021F001 is the first footprint in scan line 21.

Name	Description (Units)	Dim.	Offset
CO2 MMR	Carbon dioxide volume mixing ratio (ppb)	R4	76
T AIR	Air temperature at level (K)	100R4	156
H2O CD	Water vapor layer amount (molecules/cm^2)	100R4	556
O3 CD	Ozone layer amount (molecules/cm^2)	100R4	956
LW CD	Liquid water/ice layer amount (molecules/cm^2)	100R4	1356
Cloud Ice	Flag set to 1 when liquid water/ice is ice e	100I4	1756
CO CD	Carbon monoxide layer amount (molecules/cm^2)	100R4	2156
CH4 CD	Methane layer amount (molecules/cm^2)	100R4	2556

Table 13: The atmospheric profiles contained in the simulation. Temperatures are level values, constituents are layer amounts between the reported level and the level above. All profiles are on the pressure grid (pobs) contained in the header record.

Name	Description (Units/Range)	Dim.	Offset
Cld Frac	Viewed cloudiness (0-1.0)	2R4	125
P Cldtop	Cloud top pressure (hPa)	2R4	117
P Cldbot	Cloud base pressure, stored rspare(1:2) (hPa)	2R4	4444
NCld	Number of cloud layers (1-2)	I4	81
CLd NHinge	Number of cloud emissivities (1-7)	I2	146
Cld Freq	Cloud emissivity frequencies (cm^{-1})	7×2R4	2956
Cld Emis	Cloud emissivities (0-1.0)	7×2R4	4212
Cld Rho	Cloud reflectivities (0-1.0)	7×2R4	4268
True Cld Frac	True cloud fraction of layer 2, stored in rspare(5)	R4	4460

Table 14: Cloud properties contained in the simulation. Frequencies, emissivities and reflectivities are defined separately for each cloud layer.

Name	Description (Units)	Dim.	Offset
Topog	Mean elevation above sea level of footprint (m)	R4	52
Topog Err	Standard deviation of elevation in footprint (m)	R4	56
Land Frac	Fraction of footprint on land (0-1.0)	R4	60
Land Frac Err	Uncertainty in land fraction primarily from DEM resolution (0-1.0)	R4	64
P Surf	Surface pressure (hPa)	R4	68
T Surf	Surface skin temperature (K)	R4	72
MW Surf Class	Microwave surface class (1-6)	I1	80
Emiss MW 0	Reference microwave surface emissivity at 50.3 GHz (0-1.0)	R4	85
Emiss MW Std	Microwave surface emissivities hinge points (0-1.0)	7R4	89
Sun Glint Dist.	Distance from point where sun glint is greatest(km)	I2	141
Num Hinge Pts.	Number Of IR Surface Emissivity Hinge Points	I2	144
Freq Emis	IR Surface Emissivity Hinge Point Frequencies (cm^{-1})	100R4	2956
Emis IR	IR Surface Emissivities (0-1.0)	100R4	3356
Rho IR	IR Surface Reflectivities (0-1.0)	100R4	3756
IR Surf Class	IR Surface Class, stored in ispare(2), (0-9)	I4	4328
Albedo	Forecast visible surface albedo, stored in rspare(3), (0-1.0)	R4	4452
NDVI	Normalized differential vegetation index, stored in rspare(4), (0-1.0)	R4	4456
IR Mat Contr	Fraction of footprint covered by material i, stored in rspare(6:12), (0-1.0)	7R4	4464

Table 15: Surface properties contained in the simulation. The microwave surface emissivities at 50.3 GHz is duplicated for backward compatibility.

B NCEP Aviation Forecast Output

The NCEP aviation global analyses and forecast output files are in WMO gridded binary (GRIB) format. A GRIB record is composed of 4 sections and a terminating string '7777'. These are an indicator section, defining the length and version of the grib record, a product definition section describing the parameter contained in the record, a grid description section describing the grid, and the binary data section containing the actual data.

Fields are characterized by their parameter identifier and level contained in the parameter description section. Possible ID are tabulated in Table 2 NCEP Office Note 388 [Dey, 1998]. A level can be a pressure level, a normalized pressure (sigma) level, a layer quantity or one of the special levels such at the surface, tropopause or cloud boundary; these are tabulated in Tables 3 and 3a of Office Note 388. Profile quantities are constructed from multiple reports with the same report ID, and similar level descriptors.

The GRIB specification allows for a variety of grids, but all grids in the aviation output files are spherical latitude-longitude grids, with 1°resolution. They having 181 rows starting from 90° N and 360 columns, starting 0° E going eastward.

At the start of each run of the forecast, an objective analysis is run on the 6 hour forecast from the previous run. The resulting fields are a subset of the forecast. Table 16 list the fields common to the analysis and forecast. Table 17 list reports contained only in forecast. Some parameters have additional levels in the forecasts and this is noted in Table 17. The cloud top temperature and pressure and cloud bottom pressure fall into this category. The output files contain parameters characteristic of sub grid scale processes which are parameterized in the model, but are diagnostic of local variability. These may prove useful in validation studies to assess error sources which arise from spatial heterogeneity.

Parameter ID	Description (Units)	Levels	Range (hPa)	Used
4LFTX	Best 4-layer Lifted index (K)	(2)		
5WAVA	5-wave geopotential height anomaly (gpm)	1		
5WAVH	5-wave geopotential height (gpm)	1		
ABSV	Absolute vorticity (1/s)	26	1000-10 hPa	
CAPE	Convective available potential energy (J/kg)	(2)		
CIN	Convective inhibition (J/kg)	(2)		
GPA	Geopotential height anomaly (gpm)	2		
HGT	Geopotential height (gpm)	26(3)	1000-10 hPa	Y
HPBL	Planetary boundary layer height (m)	(1)		
ICEC	Ice cover flag (1 -¿ ice)	(1)		
LAND	Land cover (0-1.0)	(1)		
LFTX	Lifted index (K)	(2)		
O3MR	O_3 MMR (kg/kg)	6	100 - 10 hPa	Y
POT	Potential temperature (K)	(1)		
PRES	Pressure (Pa)	(5)		Y
PRMSL	Pressure reduced to sea level (Pa)	(1)		
PWAT	Precipitable water (kg/m^2	(1)		
RH	Relative humidity (%)	21(8)	1000-100 hPa	Y
SOILW	Volumetric soil moisture (0-1.0)	(2)		
SPFH	Specific humidity (kg/kg)	(2)		
TCDC	Total cloud cover (0-1.0)	(1)		Y
TMP	Temperature (K)	26(11)	1000-10 hPa	Y
TOZNE	Total ozone (Dobson)	(1)		
UGRD	Zonal wind (m/s)	26(8)	1000-10 hPa	
VGRD	Meridional wind (m/s)	26(8)	1000-10 hPa	
VSSH	Vertical speed shear [1/s)	(1)		
VWSH	Vertical wind shear [1/s)	(1)		
VVEL	Pressure vertical velocity (Pa/s)	21(1)	1000-100 hPa	
WEASD	Accumulated snow (kg/m^2)	(1)		

Table 16: Reports common to analysis and forecast output files. The first column is the parameter identifier , the second contains a brief description and the units. The third column is the number of levels, separated into the number of pressure levels and the remaining levels in parentheses. The range is the extend of profile contained on pressure levels, and the last column indicates whether any of the reports are used in the simulations.

Parameter ID	Description (Units)	Levels	Range (hPa)	Used
ACPCP	Convective precipitation (kg/m^2)	(1)		
ALBDO	Surface albedo (%)	(1)		Y
APCP	Total precipitation (kg/m^2)	(1)		
CFRZR	Categorical freezing rain flag (1-¿yes)	(1)		
CICEP	Categorical ice pellets (1-¿yes)	(1)		
CPRAT	Convective precipitation rate (kg/m^2/s)	(1)		
CRAIN	Categorical rain flag (1-¿yes)	(1)		
CSNOW	Categorical snow (1-¿yes)	(1)		
CWORK	Cloud work function (J/kg)	(1)		
DLWRF	Downgoing LW radiation (W/m^2)	(1)		
DSWRF	Downgoing SW radiation (W/m^2)	(1)		
GFLUX	Ground heat flux (W/m^2)	(1)		
LHTFL	Net latent heat flux (W/m^2)	(1)		
PEVPR	Potential evaporation rate (W/m^2)	(1)		
PRATE	Precipitation rate (kg/m^2/s]	(1)		
PRES	Average Cloud Top Pressure (Pa)	(3)		Y
PRES	Average Cloud Bottom Pressure (Pa)	(3)		Y
SHTFL	Net sensible heat flux (W/m^2)	(1)		
TMP	Cloud top temperature (K)	(3)		
TCDC	Total cloud cover (%)	(6)		Y
TMIN	Minimum surface air temperature (K)	(1)		
TMAX	Maximum surface air temperature (K)	(1)		
UFLX	Zonal momentum flux (N/m^2)	(1)		
U-GWD	Zonal gravity wave stress (N/m^2)	(1)		
ULWRF	Upward LW Radiation Flux (W/m^2)	(2)		
USWRF	Upward SW Radiation Flux (W/m^2)	(2)		
V-GWD	Meridional gravity wave stress (N/m^2)	(1)		
VFLX	Meridional momentum flux (N/m^2)	(1)		
WATR	Water runoff (kg/m^2)	(1)		

Table 17: Reports contained in forecast files only. The columns are as described for Table 16.

C Acronyms

Acronym	Description
ACRS	AIRS Core Product Retrieval System
AIRS	Atmospheric InfraRed Sounder
AIRSBT	AIRS Level 1B simulator (Brightness Temperature)
AL2SS	AIRS Level 2 Simulation System
AMSU	Advanced Microwave Sounding Unit
AMSU-A1	AMSU unit A, module 1 (O_2 and 89 GHz channels)
AMSU-A2	AMSU A, module 2 (23.8 and 31.4 GHz channels)
AMSU-B	AMSU unit B, POES microwave humidity sounder, functionally similar to HSB with 1 additional channel
ATMOS	Atmospheric Trace MOlecule Spectroscopy experiment
AVHRR	Advanced Very High Resolution Radiometer
AvnSim	AIRS Level 2 Simulations System (acronym from AViatioN SIMulations)
CERES	Clouds and the Earth's Radiant Energy System
DGM	Digital Geography Model
ECS	EOS Core System
EOS	Earth Observing System
ESDP	EOS Science Data Processing
FOV	Field of View
GeoSim	Geolocation Simulator
HIRS	High-resolution InfraRed Sounder
HSB	Humidity Sounder Brasil (functionally identical to AMSU-B)
IGBP	International Geosphere Biosphere Programme
MLS	Microwave Limb Sounder
NDVI	Normalized Differential Vegetation Index (for AVHRR $\frac{B_2-B_1}{B_2+B_1}$)
PGE	Process Generation Executive
POES	NOAA Polar Oribiting Environmental Satellite
PM1ATTN	EOS PM 1 platform (Aqua) ATTitude, Nominal file
PM1EPHP	EOS PM 1 platform (Aqua) EPHemeris, Predicted file
RadSim	Radiance Simulated Products
RTA	Rapid Transmission Algorithm
TLSCF	AIRS Team Leader Science computing Facility
UARS	Upper Atmosphere Research Satellite